Crack Propagation in Decagonal and Icosahedral Quasicrystals

Von der Fakultät Mathematik und Physik
der Universität Stuttgart
zur Erlangung der Würde eines Doktors der
Naturwissenschaften (Dr. rer. nat.) genehmigte Abhandlung

Vorgelegt von

Christoph Paul Rudhart

aus Friedrichshafen

Hauptberichter : Prof. Dr. Hans-Rainer Trebin
Mitberichter : Prof. Dr. Hans Herrmann

Tag der mündlichen Prüfung : 23.02.2004

Institut für Theoretische und Angewandte Physik
Universität Stuttgart

2004

Contents

Zusammenfassung

Die vorliegende Arbeit beschäftigt sich mit der atomistischen Simulation der Rissausbreitung in Quasikristallen. Quasikristalle – 1984 von Shechtman und Mitarbeitern [1] entdeckt – stellen eine neue Klasse geordneter Festkörper dar. Sie zeigen Beugungsmuster mit scharfen Bragg-Reflexen, die jedoch mit nichtkristallographischen Symmetrien verbunden sind. Das Auftreten scharfer Bragg-Reflexe weist auf eine weitreichende Translationsordnung hin. Dadurch unterscheiden sich Quasikristalle von amorphen Festkörpern. Darüber hinaus sind nichtkristallographische Symmetrien nicht vereinbar mit einem periodischen Aufbau der zugrundeliegenden Struktur. Daher lassen sich Quasikristalle nicht durch periodische Anordnung einer Einheitszelle beschreiben.

Bedingt durch ihre quasiperiodische Struktur treten in Quasikristallen strukturelle Defekte auf, die in periodischen Kristallen nicht vorkommen. Beispielsweise hinterlassen Versetzungen in Quasikristallen stets Stapelfehler, die als Phasonenwände bezeichnet werden. Ein weiteres Charakteristikum von Quasikristallen sind globulare Atomanordnungen, so genannte Cluster, die die Bewegung von Versetzungen behindern. In der vorliegenden Arbeit wird der Einfluss der quasiperiodischen Ebenenstruktur und der Cluster auf die Mechanismen der Rissausbreitung dekagonaler und ikosaedrischer Quasikristalle unter öffnender Belastung untersucht.

Im Rahmen der linear elastischen Bruchmechanik werden Risse als freie innere Grenzflächen behandelt. Diese idealisierte Beschreibung ist aus zwei Gründen problematisch. Zum einen liefert die Modellierung durch scharfe Risse unendlich hohe Spannungskonzentrationen an der Rissspitze. Daher verliert die linear elastische Bruchmechanik in der unmittelbaren Umgebung der Rissspitze ihre Gültigkeit. Andererseits können Effekte, deren Ursprung in der diskreten Natur der Materie liegen, nicht mit Kontinuumstheorien beschrieben werden. Daher wurde in der vorliegenden Arbeit die Methode der Molekulardynamik eingesetzt, um speziell die atomistischen Effekte der Rissausbreitung in Quasikristallen zu studieren.

Das Auftreten von Rissen resultiert in Spannungsfeldern mit langer Reichweite. In Molekulardynamik lässt sich nur eine endliche Anzahl von Atomen behandeln. Daher muss bei der atomistischen Modellie-

rung der Rissausbreitung insbesondere auf die Wahl geeigneter Randbedingungen geachtet werden. In der vorliegenden Arbeit wurde eine Streifengeometrie gewählt, die es erlaubt, Rissausbreitung mit konstanter Energiefreisetzungsrate zu studieren. Hierbei wird in einen langen Streifen das Verschiebungsfeld eines Risses eingebracht und anschließend relaxiert. Durch Skalierung des Verschiebungsfeldes um den stabilisierten Riss wird die Probe belastet und die Antwort des Systems in Molekulardynamik verfolgt.

Zur Simulation der Rissausbreitung bei höheren Temperaturen wurde ein neues Verfahren entwickelt [2]. Es ist an einen experimentellen Aufbau angelehnt, der häufig zur Untersuchung des Spröd-Duktil-Übergangs angewendet wird. Ein langer Streifen wird mit einem Temperaturgradienten versehen. Der Riss wird in einem Gebiet mit tiefer Temperatur stabilisiert und durch die angelegte Belastung entlang des Gradienten getrieben, bis er zum Stillstand kommt. Mit Hilfe dieses Verfahrens lassen sich Risse über weite Temperaturbereiche simulieren und so die Änderungen der Ausbreitungsmechanismen mit steigender Temperatur verfolgen.

Dekagonale Quasikristalle besitzen eine quasiperiodische Ordnung in zwei Raumrichtungen und eine periodische Ordnung senkrecht dazu. In der vorliegenden Arbeit wird die Rissausbreitung in zweidimensionalen Modellquasikristallen simuliert.

Die Mechanismen der Rissausbreitungen lassen sich grob in drei unterschiedliche Temperaturbereiche einteilen:

Für tiefe Temperaturen – bis 30% der Schmelztemperatur T_m – tritt in Quasikristallen ein neuartiger Ausbreitungsmechanismus [3] auf. Dabei wird von der Rissspitze ein Versetzung auf einer Gleitebene emittiert, die um 36° gegenüber der Spaltebene verkippt ist. Durch die quasiperiodische Struktur zieht die Versetzung einen Stapelfehler nach sich. Entlang des Stapelfehlers ist die Kohäsivenergie der Struktur reduziert, und der Riss folgt der Versetzung. Während in periodischen Kristallen emittierte Versetzungen die Rissspitze abstumpfen und die Rissausbreitung behindern, fördern sie den Sprödbruch in den untersuchten Modellquasikristallen.

Im Bereich von 30%-70% T_m wird ein spontanes Abstumpfen der Rissspitze durch Versetzungsemission beobachtet. Im Gegensatz zum Tieftemperaturbereich nukleiert hier eine Versetzung auf einer gegenüber der Spaltfläche um 72° geneigten Gleitebene. Für niedrige Belastungen ist die Versetzung in der Lage, den Riss von der äußeren Belastung abzuschirmen, was zum Rissstillstand führt.

Im Hochtemperaturbereich wechselt der Mechanismus. Wird die Rissausbreitung bei tiefen Temperaturen durch die Ebenenstruktur und die globularen Strukturen dominiert, so erfolgt sie bei hohen Temperaturen $T > 0.70\,T_m$ durch Wachstum und Koaleszenz mikroskopischer Poren vor der Rissspitze. Dieses Porenwachstum ist mit plastischer Verformung vor der Rissspitze verbunden. Eine detaillierte Analyse der Atompositionen vor der Rissspitze zeigt, dass die plastische Verformung durch Atomumordnungen bedingt ist. Diese treten in streng lokalisierten Bereichen um die Rissspitze auf. Ähnliche Umordnungsprozesse wurden in Simulationen der plastischen Verformung und der Rissausbreitung in nichtkristallinen Modellsystemen beobachtet. Diese so genannten Schertransformationszonen wurden als Mechanismus der plastischen Verformung von Gläsern vorgeschlagen und bilden die Basis für Modelle der viskoplastischen Verformung amorpher Festkörper.

Ikosaedrische Quasikristalle weisen eine quasiperiodische Ordnung in allen drei Raumrichtungen auf. Daher lässt sich die Rissausbreitung nicht auf zweidimensionale Modellsysteme reduzieren. Das in der vorliegenden Arbeit verwendete Strukturmodell wurde von Henley für die ikosaedrische Phase von AlZnMg vorgeschlagen.

In der vorliegenden Arbeit wurden Risse auf Spaltebenen senkrecht zu zwei- und fünfzähligen Spaltebenen untersucht. Wie bei den dekagonalen Modellen ist die Rissausbreitung bei tiefen Temperaturen durch spröden Spaltbruch gekennzeichnet. In periodischen Kristallen spielt die Orientierung der Bruchebene gegenüber den Gleitsystemen eine entscheidende Rolle. Um den Einfluss der Gleitebenenorientierung zu untersuchen haben wir die Orientierung der Risse variiert. Im Gegensatz zu den Simulationen in dekagonalen System wurde jedoch unabhängig von der Orientierung der Spaltebene und der Rissausbreitungsrichtung keinerlei Anzeichen für die Emission von Versetzungen beobachtet.

Die beobachteten Bruchflächen zeigen eine ausgeprägte Rauigkeit. Um die Morphologie der Bruchflächen zu studieren haben wir die atomistischen Rissufer selektiert und geometrisch – ähnlich wie bei einem Rasterkraftmikroskop – abgetastet. Die Rauigkeit hängt hierbei von der Wahl der Spaltflächen und der Ausbreitungsrichtung ab. Zudem treten bei Simulationen auf der gleichen Spaltebene bei Ausbreitung *senkrecht* zu einer zweizähligen Richtung Stufen auf, die bei Ausbreitung *parallel* zu dieser Richtung nicht beobachtet werden. Insbesondere die Abhängigkeit von der Ausbreitungsrichtung ist aus kontinuumsmechanischer Sicht nicht erklärbar.

Ebert et al. [4] haben ikosaedrische AlPdMn-Einquasikristalle im Ultrahochvakuum gespalten und die Bruchflächen mit Rastertunnel- und Rasterelektronenmikroskopie untersucht. Die Spaltflächen sind mit globularen Strukturen bedeckt und somit rau. Dies legt nahe, dass die beobachtete Rauigkeit durch die in der Struktur enthaltenen Cluster verursacht wird. Molekulardynamische Studien erlauben es, die Trajektorie jedes einzelnen Atoms während der Simulation zu verfolgen. Dadurch ist es nicht nur möglich zu untersuchen, ob der Riss die in der Struktur enthaltenen Cluster durchtrennt, es kann auch festgestellt werden, wie die Cluster durchschnitten werden. Eine detaillierte Analyse der durchtrennten Cluster zeigt deutlich, dass diese durch den Riss nicht strikt umlaufen, sondern zu einem gewissen Grad durchschnitten werden. Die Cluster werden jedoch weniger häufig durchtrennt, als dies bei einem ebenen Schnitt der Fall wäre. Dies legt die Vermutung nahe, dass die Morphologie der Bruchflächen in der Tat durch die in der Struktur enthaltenen Cluster beeinflusst wird.

Die Simulationen auf fünfzähligen Spaltebenen zeigen, dass der Riss von der ursprünglichen Spaltebene abweicht und sich auf einer dazu parallelen Ebene ausbreitet. Dieses Verhalten kann wiederum mit dem Auftreten der Cluster erklärt werden. Bei den Simulationen wurde der Riss auf einer Ebene mit niedriger Oberflächenenergie eingebracht. Die Verteilung der Cluster wurde hierbei nicht berücksichtigt. Der Riss weicht auf eine parallele Ebene aus und minimiert so die Zahl der durchtrennten Cluster.

Die Simulationen zeigen, dass die komplexen Phänomene der Rissausbreitung in Quasikristallen nicht durch Kontinuumstheorien verstanden werden können. Insbesondere der Einfluss der in den Strukturen enthaltenen globularen Strukturen kann nur mit Hilfe atomistischer Modelle erfasst werden.

Chapter 1

Introduction

In 1984 Shechtman et al. [1] reported on the discovery of a metastable phase of an AlMn alloy with a diffraction pattern of sharp Bragg peaks with crystallographically forbidden rotational symmetries. The appearance of sharp Bragg-peaks clearly indicated that the new phase showed long range translational order. Thus it could be clearly distinguished from amorphous structures. On the other hand are crystallographically forbidden rotational symmetries incompatible with periodicity. It followed that the new phase could not be periodically ordered like ordinary crystals. It is now commonly accepted that this was the discovery of a new type of ordered solids, which were termed quasicrystals. This discovery of an ordered structure without translational periodicity provided a challenge to solid state physicists since many traditional concepts rely on translational periodicity. As an example, most atomistic models to predict the response of a material to an external load are based on the periodicity of the underlying structure, and thus do not directly apply to quasicrystals.

Materials are often classified as brittle if they shatter like glass and ductile if they are deformable. Whereas perfectly brittle materials fail without significant plasticity, ductile failure is associated with large plastic deformations. In experiments, quasicrystals show a pronounced brittle to ductile transition (BDT) that occurs at high homologous temperatures of about 80% of the melting temperature. Whereas different models exist for the BDT in crystalline materials, it is less well understood in amorphous or quasicrystalline materials. On the macroscopic scale the BDT is a complicated phenomenon that depends not only on the material under consideration and the temperature but also on the loading rate and the microstructure of the solid. Obviously a phenomenon in which processes on many different length scales are involved cannot be understood merely by atomistic models. However, like in crystalline materials, the macroscopic changes should be a consequence of processes that occur essentially on the atomic scale.

The current work focuses on the atomistic aspects of fracture in quasicrystals. Crack propagation in two-dimensional decagonal and three-

dimensional icosahedral model quasicrystals is studied by means of molecular dynamics simulations which have proven a powerful tool to understand the basic features of the fracture process in periodic crystals. One key property of quasicrystals is the occurrence of tightly bound atomic clusters. In molecular dynamics simulations it is possible to follow the trajectory of each individual atom in a multi-particle system. Thus molecular dynamics is particularly suitable to study the influence of the clusters on the modes of crack propagation in quasicrystals. The aim of the current work is to contribute to a better understanding in which way the modes of crack propagation in quasicrystals are influenced by their peculiar structure.

The work is divided into three parts. The first part contains a short introduction to quasicrystals and the results of fracture mechanics that are important for modeling of crack propagation by means of molecular dynamics simulations. The boundary conditions and integration schemes used to model crack propagation at finite temperatures are presented in detail.

The second part is devoted to the simulations in two-dimensional decagonal model quasicrystals. The aim of the studies is to contribute to a better understanding of the influence of the temperature on the modes of crack propagation in decagonal quasicrystals. Earlier simulations of the fracture of quasicrystals have been performed at low temperatures, where quasicrystals fail by brittle fracture [3, 5, 6]. Fracture at higher temperatures and the BDT have not been studied yet. Here molecular dynamics simulations are applied to study the dynamic crack propagation in a wide range of temperatures to elucidate the atomic features that are important for the understanding of the BDT in decagonal quasicrystals.

The third part contains the results of a series of simulations of crack propagation in a three-dimensional icosahedral model systems. Investigations of cleavage surfaces in icosahedral quasicrystals by scanning tunneling microscopy clearly show that the structure of fracture surfaces [4] is strongly influenced by clusters that are inherent in the structure. This part focuses on the brittle fracture at low temperatures and

on the influence of the clusters on the morphology of the fracture surfaces in particular.

Although the models used in the current work are simple, they display the main characteristics of quasicrystals. Thus the simulations might give an indication of the characteristic features and the elementary processes that dominate the fracture process in real quasicrystals.

Chapter 2

Quasicrystals

2.1 Introduction

Periodic crystals can be described as an arrangement of atoms in a unit cell which is repeated periodically. The crystal structure is defined by the unit cell and the lattice structure. This yields a long-range translational and orientational order of the atomic structure. Periodic arrangements admit only rotational axis with one-, two-, three-, four-, and sixfold symmetry. In classical 3d crystallography rotational symmetries with fivefold, sevenfold or higher rotational symmetries are excluded and termed crystallographically forbidden symmetries.

In 1984 Shechtman et al. reported the discovery of a metastable phase of a AlMn alloy with a diffraction pattern of sharp spots that showed such crystallographically forbidden rotational symmetries [1]. They observed twofold, threefold and fivefold symmetries according to the icosahedral point-group. Due to the sharp diffraction spots the structure has to possess a long-range order. Thus, the structure could not be amorphous. However, a periodic arrangement of atoms could be excluded by the symmetry of the system. It is now commonly accepted that this was the discovery of a new class of solids, which are defined as structures with long-range aperiodic order and crystallographically forbidden rotational symmetries. These materials are named quasicrystals by Levine and Steinhardt [7] as a shortened form of quasiperiodic crystal.

There are three different classes of quasicrystals:

- **One-dimensional quasicrystals:** They are given by quasiperiodic stackings of periodic planes. Examples are AlCuMn,AlNiSi [10], and AlPd [11].
- **Two-dimensional quasicrystals or T-Phases:** They consist of periodic stackings of aperiodic layers of atoms. Within this group there exist different types that are named by the symmetry of the quasiperiodic layers. There are decagonal quasicrystals with a tenfold rotational axis, like AlNiCo or AlCuCo, octagonal with eightfold [12] or dodecagonal [13] quasicrystals with twelvefold symmetry.

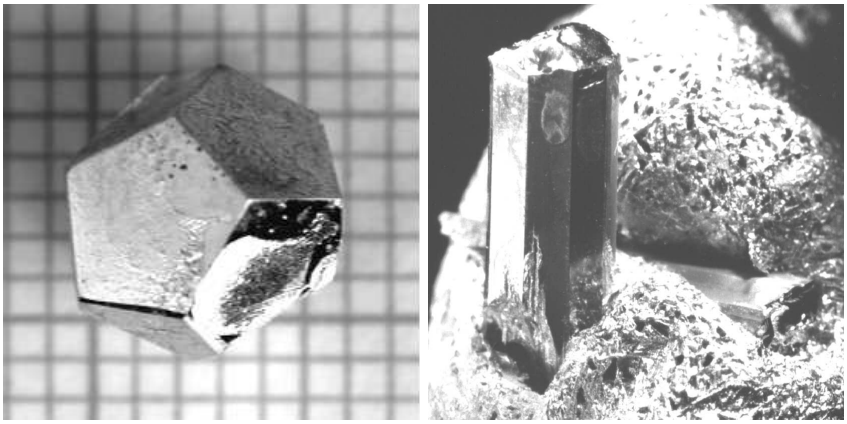

Figure 2.1: *Centimeter sized icosahedral ZnMgDy [8](left) and decagonal AlNiCo [9] (right) single quasicrystal.*

- **Three-dimensional or icosahedral quasicrystals**: Icosahedral quasicrystals show quasiperiodicity in all three spacial directions with icosahedral symmetry. The first quasicrystals that were observed in the AlMn system belong to that class. Other examples are icosahedral AlPdMn, AlCuLi and AlCuFe.

Since their discovery a large number of thermodynamically stable quasicrystals were found in many different alloy systems. They can be roughly classified as aluminum based quasicrystals like AlPdMn [14], AlCuLi [15,16] or AlCuFe [17], rare earth quasicryals like ZnMgDy [18] and Ti-based quasicrystals like TiZrNi [19].

The first thermodynamically stable quasicrystal was found in the AlCuLi system [15]. Whereas the first stable phases could only be grown as polycrystals with grains of only millimeter-size, nowadays large single quasicrystals of cubic centimeter-size [20] are available. Examples of centimeter-sized decagonal AlNiCo [9] and icosahedral ZnMgDy [8] single quasicrystals are shown in Fig. 2.1. The forbidden five- and tenfold symmetries are also present in the growth morphology. An overview of the single quasicrystal growth techniques is given in [8].

Up to very recently all stable quasicrystals were found in ternary systems. However, binary quasicrystals were discovered recently in CdCa and CdYb [21].

Quasicrystalline materials show a number of remarkable properties including high heat capacity, low heat conductivity [22] and a very large electrical resistivity [23]. This is especially remarkable because they consist of the same elements as conventional intermetallic compounds. Some of the properties may be attractive for technological applications [24].

2.2 Mechanical Properties

The behavior of single quasicrystals under mechanical loads has been the subject of numerous studies in the last years (for reviews, see [25] and [26]). The main results are a pronounced brittle to ductile transition (BDT) at about 80% of the melting temperature T_m and a good deformability up to 20% without hardening above the BDT. These properties are attributed to the peculiar structure of quasicrystals. On the one hand, quasicrystals are cluster-based structures. The clusters act as obstacles to moving dislocations which are responsible for the plastic deformation. On the other hand, quasicrystals possess a quasiperiodic plane structure. As a result moving dislocations are always followed by planar defects, so-called phason walls [27]. The phason walls and the clusters are believed to play the main parts in the process of plastic deformation.

In contrast to the plasticity of quasicrystals, experiments on crack propagation in single quasicrystals are scarce. Most are indentation tests in which the fracture toughness is estimated from the geometry of the indentations, the applied external force, and the length of the microcracks emitted from the indenter corners [28]. The values for the fracture toughnesses at room temperature are about $1 MPam^{1/2}$ [28, 29] which is close to those for brittle ceramics or silicon [30]. The cracks in the vicinity of microhardness indentations are observed to propagate predominantly along well-defined crystallographic planes [28]. Investigations of cleavage surfaces by scanning tunneling microscopy clearly show that the structure of fracture surfaces [4] is influenced by clusters.

However, the atomistic scale is not accessible to experiments if the dynamics of the fracture process is concerned.

2.3 Quasiperiodic Structures

Quasicrystals are defined as ordered atomic structures that exhibit long-range quasiperiodic translational and long-range orientational order with disallowed crystallographic symmetry [31]. Thus, quasicrystals cannot be constructed by periodic repetition of a single atom or a single unit cell. However, they can be obtained by decorations of a so-called quasilattice or quasiperiodic tiling that contain two ore more unit cells.

A tiling is an arrangement of a finite number of different polygons in two dimensions or polyhedra in three dimensions, so-called tiles, which fills the underlying space without overlaps or gaps. The model quasicrystals used in the present work are exclusively decorations of such tilings.

There are different methods to generate quasiperiodic tilings (for a review see [31]). One possibility is the so-called cut and projection [32,33] or strip projection method [34]. The main idea is to generate quasiperiodic tilings as projections from higher-dimensional spaces. The crystallographically forbidden point groups that appear in quasiperiodic tilings are symmetry groups of higher-dimensional periodic lattices. By projecting a subset of the higher-dimensional lattice into an appropriate subspace one can achieve that the resulting point set forms the vertices of a quasiperiodic tiling.

In the following the method is described for the simplest nontrivial example, the one-dimensional Fibonacci-chain, and then is extended to the two- and three-dimensional case to construct the quasiperiodic tilings that form the basis for the model quasicrystals used in the current work.

We start from the two-dimensional square lattice $\mathbb{Z}^2$ in the plane $\mathbb{R}^2$ (see Fig. 2.2). The line through the origin $y = mx$, embedded in the plane is called parallel space $E^{\parallel}$ or physical space in the following. The line through the origin perpendicular to $E^{\parallel}$ with slope $-1/m$ is called perpendicular space $E^{\perp}$ or internal space.

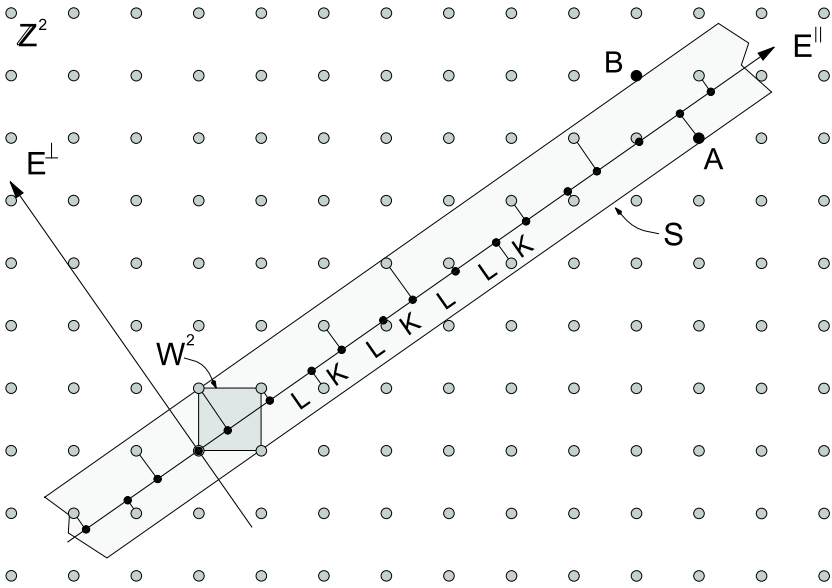

Figure 2.2: *Cut and project method for the one-dimensional Fibonacci-chain.*

Consider now the strip S obtained by shifting the unit square W^2 along $E^{\parallel}$. By projecting the subset of points from $\mathbb{Z}^2$ that are within the strip[1] orthogonally on $E^{\parallel}$, one obtains a sequence of long (L) and short (S) segments. If the slope m is chosen to be irrational, the sequence is not periodic but quasiperiodic. For the case $m = \tau^{-1}$ where $\tau = (1+\sqrt{5})/2$ is the golden mean, the resulting sequence is given by the well-known Fibonacci-chain. The orthogonal projection of S on $E^{\perp}$ is called the acceptance domain or window of the tiling. The shape of the acceptance domain determines which points are projected.

The orthogonal projections of the unit vectors e_0 and e_1 of $\mathbb{Z}^2$ are given by two vectors a_0, a_1 with lengths of the segments L and S respectively. The aspect ratio of L and S is given by τ. The vectors a_i form a basis

[1]By projecting only the points that lie within the strip the resulting sequence shows gaps. Therefore the strip is defined as a half-open region where only the poins on one side of the strip are projected.

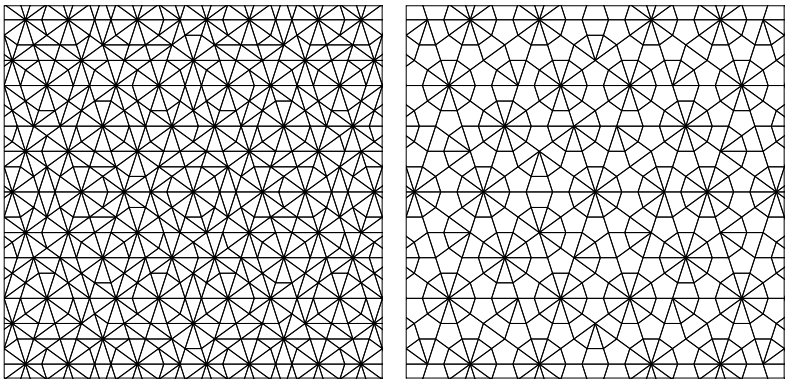

Figure 2.3: *Tübingen triangle tiling (left) and simplified tiling.*

of the quasiperiodic sequence. Each point can be described uniquely by an integer linear combination of the basis vectors a_0 and a_1. Although the physical space is one-dimensional, two basis vectors are needed to write each point as such an integer linear combination. This is one of the properties that distinguish quasiperiodic lattices from periodic ones. For quasiperiodic lattices the rank of the basis always exceeds the dimension of the physical space.

For the Fibonacci-chain the slope was chosen to be irrational. In the case of a rational slope m the resulting sequence is periodic. By choosing a rational approximation of the inverse golden mean one obtains a sequence that is called a rational approximant. The better the slope approximates the inverse golden mean the better is the approximation of the quasiperiodic sequence.

Some simulation techniques that were performed in the current work require periodic boundary conditions. For this purpose periodic approximants were used instead of perfectly quasiperiodic structures. However, the difference between the approximant and the perfectly quasiperiodic structure is small, at least if the unit cell of the approximant is chosen to be large compared to the cut-off radius of the potential.

The Tübingen triangle tiling [35] is obtained by projection from the four-dimensional root lattice[2] $\mathbb{A}^4$, which is a sublattice of the five-dimensional simple cubic lattice $\mathbb{Z}^5$. However, the lattice $\mathbb{Z}^5$ is more intuitive as a starting point. Thus we construct the tiling as a projection of the $\mathbb{Z}^5$ with basis vectors $e_i (i = 0, \cdots, 4)$. The physical space $E^{\parallel}$ and the orthogonal space $E^{\perp}$ are given by twodimensional subspaces of $\mathbb{R}^5$.

The acceptance domain is constructed from the Voronoi cell of the root lattice $\mathbb{A}^4$. The projection of the Voronoi cell into the perpendicular space $E^{\perp}$ forms the acceptance domain which is given by a regular decagon. The vertices of the Tübingen triangle tiling are obtained by orthogonal projection of a subset of the vertices of $\mathbb{A}^4$ into the physical space $E^{\parallel}$. Just like in the two-dimensional case a point is projected only if its orthogonal projection lies within the acceptance domain. Fig. 2.3 shows a section from the Tübingen triangle tiling. It consists of two different tiles, an acute and an obtuse triangle. As in periodic lattices each vertex of the tiling can be written as an integer linear combination of the basis vectors $g_i (i = 0, \cdots, 4)$ which are the orthogonal projections of the e_i in $E^{\parallel}$. The vectors g_i point to the vertices of a regular pentagon. Although this is not a minimal basis, since any four of the e_i already form a basis, all five vectors are often used for convenience.

It should be noted here that the projection method as it is described above only allows to construct the vertices of the triangle tiling but not the entire set of the edges. This results in a simplified version of the Tübingen triangle tiling that consists of three different tiles, an acute triangle, a regular pentagon and a trapezoid (see Fig. 2.3). However, the vertices are sufficient to construct the binary model quasicrystal that is used in the current work. The construction of the complete Tübingen triangle tiling is described in [36].

The three-dimensional Ammann-Kramer-Penrose tiling also called the three-dimensional Penrose tiling is constructed from the six-dimensional simple cubic lattice $\mathbb{Z}^6$. Both, the physical space $E^{\parallel}$ and the orthogonal space are three-dimensional subspaces of $\mathbb{R}^6$. The acceptance domain is given by othogonal projection of the six-dimensional unit cube W^6 into

[2]Root lattices are generalizations of the three-dimensional face centered cubic lattice.

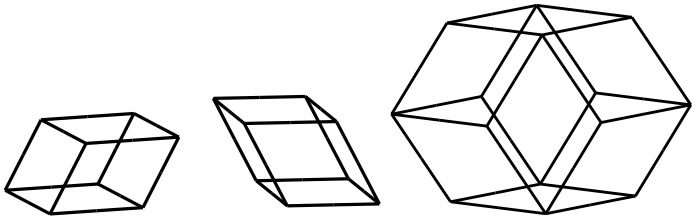

Figure 2.4: *Tiles of the Ammann-Kramer-Penrose tiling and the rhombic dodecahedron consisting of two oblate and two prolate rhomboedra.*

the orthogonal space $E^{\perp}$ and is a rhombic triacontahedron. The tiling contains two types of prototiles, an oblate and a prolat rhomboedron (see Fig. 2.4). Each vertex in the tiling can be written as an integer linear combination of basis vectors $g_i (i = 0, \cdots, 5)$ which are the orthogonal projections of the six basis vectors from Z^6. The basis vectors g_i point to the corners of a regular icosahedron. The three-dimensional Penrose tiling is used to construct the binary model quasicrystals for the fracture simulations in icosahedral quasicrystals.

2.4 Phonon and Phason Displacements

Quasicrystals carry additional degrees of freedom that do not appear in periodic crystals. These can be described by inspecting the effect of deformations of the hyperlattice in the strip projection of the Fibonacci chain depicted in Fig. 2.2. Uniform displacements that have only components in $E^{\parallel}$ lead to a rigid shift of the entire sequence. Spatial varying deformations result in distortions of the segments without changing their arrangements in the sequence. In analogy to periodic crystals such deformations are termed phonon deformations.

In contrast, a uniform displacement of the hyperlattice perpendicular to $E^{\parallel}$ does not effect the shape of the segments. Such displacements are equivalent to a shift of the strip parallel to the orthogonal space $E^{\perp}$. Consider the two points denoted by **A** and **B** in Fig. 2.2. By shifting the strip parallel along $E^{\perp}$ it happens that the point denoted by **A** in Fig. 2.2 is leaving the strip. Simultaneously, point **B** enters the strip

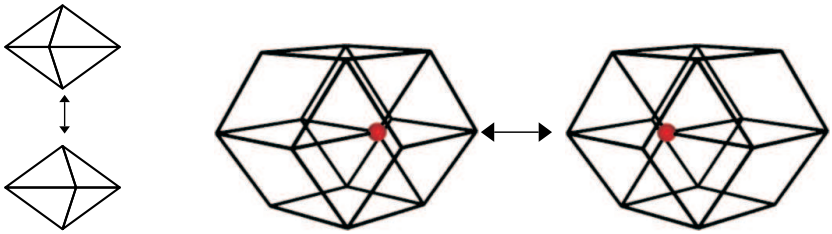

Figure 2.5: *Phason flips in the Tübingen triangle tiling (left) and the three-dimensional Ammann-Kramer-Penrose tiling (right).*

from the opposite side. This leads to a jump of the vertex associated with **A** to the position of the orthogonal projection of **B**. This jump is called a phason flip and results in a rearrangement of two segments from LS to SL in the sequence.

Since the slope of $E^{\parallel}$ is an irrational number the orthogonal projections of the lattice points of $\mathbb{Z}^2$ into $E^{\perp}$ are densly distributed along the orthogonal space $E^{\perp}$. From this it follows that, if the whole strip is displaced rigidly along $E^{\perp}$ there are infinitely many vertices that leave and enter the strip and consequently an infinitely number of phason flips along the chain. Nevertheless, the resulting tiling is physically indistinguishable from the initial tiling. However, a spatial varying displacement of the strip yields to so-called phason strain and as a result in discrete local rearrangement of tiles.

Fig. 2.5 shows flips for the Tübingen triangle tiling and the three-dimensional Ammann-Kramer-Penrose tiling. Just like in the one-dimensional case each flip consists of discrete jump of a vertex which results in a rearrangement of tiles.

The existence of the phason degrees of freedom may result in particular physical properties. For example, repeated phason flips can result in long range diffusion of vertices [37]. A model for self-diffusion based on phason flips was proposed by Katz and Kalugin [38]. Recently, thermally fluctuating phason flips have been observed in-situ by high-resolution transmission electron microscopy [39, 40]. In the current work we use phason flips to construct a two-dimensional random tiling model.

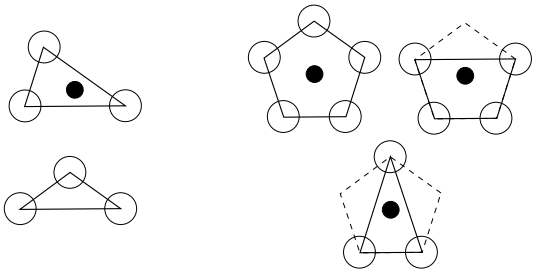

Figure 2.6: *Decoration of the tiles in the Tübingen triangle tiling (left) and the simplified tiling (right).*

2.5 Model Quasicrystals

To study crack propagation by molecular dynamics one has to choose a structure model and a suitable model for the atomic interaction. The model quasicrystals used in the current work are exclusively obtained by decoration from quasiperiodic tilings. In the following the expression tiling is used as a synonym for the atomic representation. In this section we will introduce the decorations for the model systems. The properties of the models will be discussed in Sec. 5.1 and 6.1.

2.5.1 Two-dimensional Model Quasicrystals

Decagonal quasicrystals consist of a periodic stacking of quasiperiodic planes. Thus we restrict the analysis to two-dimensional models which display the main characteristics of decagonal quasicrystals. We use two different structures, the Mikulla-Roth tiling (MRT) which is a perfectly ordered quasicrystal and a randomized model quasicrystal (RT). Both model quasicrystals are decagonal binary tilings (BT) [41, 42]. BT consist of two types of Penrose rhombs shown in Fig. 2.7 which are decorated by two species of atoms. The bond lengths fulfill the requirement that five particles of type A surround one B particle and ten B particles surround one A particle.

The Mikulla-Roth tiling (MRT) [43] is obtained from the simplified version of the Tübingen triangle tiling shown in Fig. 2.3 by placing large

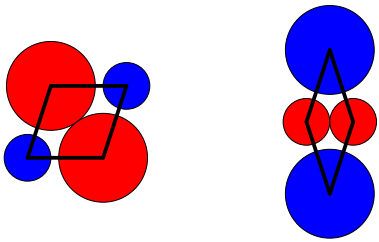

Figure 2.7: *Penrose rhombs of binary tilings and their decoration.*

(A) atoms on the vertices of the tiling and small (B) atoms on the circumcenters of the triangles, trapezoids, and pentagons as depicted in Fig. 2.6.

The randomized model quasicrystal is also constructed from the simplified Tübingen triangle tiling. Random binary tilings are defined as tilings consisting of the two different Penrose rhombs shown in Fig. 2.7. The only restriction for the arrangement of the rhombs is that at any given vertex only rhomb corners decorated with the same atom type meet. Starting from a perfectly ordered tiling the phason degree of disorder was increased through random phason flips. Sections from both model systems are depicted in Fig. 2.8.

2.5.2 Icosahedral Model Quasicrystals

In contrast to decagonal quasicrystals, icosahedral quasicrystals show quasiperiodic order in three dimensions, which cannot be reduced to simple two-dimensional model systems.

The simulations are carried out for a three-dimensional binary model quasicrystal proposed by Henley and Elser [44] as a structure model for icosahedral $(Al,Zn)_{63}Mg_{37}$. As we do not distinguish between Al and Zn, the model consists of two types of atoms, larger ones that represent Mg and smaller ones that represent Al or Zn atoms.

The system is obtained by decoration of a three-dimensional Ammann-Kramer-Penrose tiling which consists of two different tiles, oblate and prolate rhomboedra with rhombic faces. The edges are oriented parallel

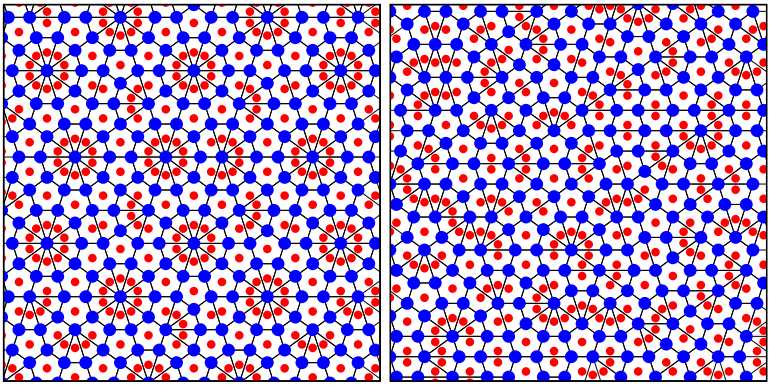

Figure 2.8: *Atomic decoration of the simplified Tübingen triangle tiling (left) and the random tiling model(right).*

to the centre-to-vertex vectors of an icosahedron. The length of the edges a_R is called the quasilattice constant.

One important structure element in the decoration is given by the rhombic dodecahedron. It consists of two oblate and two prolate rhomboedra (see Fig.2.4). The decoration consists of two steps. First neighboring pairs of two oblate rhomboedra together with two prolate rhomboedra are grouped to rhombic dodecahedra[3]. Subsequently the three prototiles are decorated as shown in figure Fig. 2.9.

Both rhomboedra are decorated by placing small atoms (A) on the vertices and the midpoints of all edges. Two large atoms (B) are placed on the long body diagonal of the prolate rhomboedron in a way that they divide the diagonal in a ration $\tau : 1 : \tau$

The rhombic dodecahedron is also decorated by placing small (A) atoms on the vertices and at the midpoint of each edge. The interiors of the rhombic dodecahedra contain eight large atoms (B) forming a slightly distorted hexagonal bipyramid (see Fig. 2.9).

[3]It should be noted that the grouping is by no means unique. The grouping was performed to maximize the number of resulting rhombic dodecahedra which is equal to minimize the number of ungrouped oblate rhomboedra.

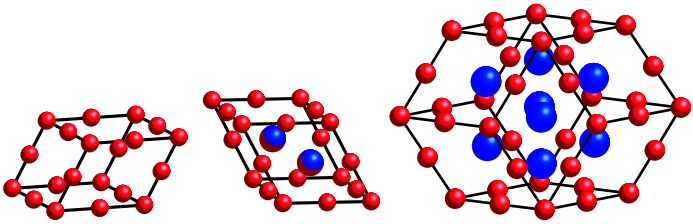

Figure 2.9: *Decoration of the Ammann-Kramer-Penrose tiling.*

2.6 Dislocations in Quasicrystals

All defects that are known from periodic crystals such as dislocations, grain boundaries or anti-phase boundaries are also observed in quasicrystals. However, quasicrystals show some additional types of defects that do not appear in periodic crystals. One example that is important for the crack propagation are the so-called phason walls that appear in connection with dislocations in quasicrystals.

Fig. 2.10 shows a schematic representation of a periodic and a quasiperiodic sequence of planes where the upper part was shifted against the lower part resulting in a plastic deformation. In the periodic structure the upper part was shifted for the separation of the planes which yields

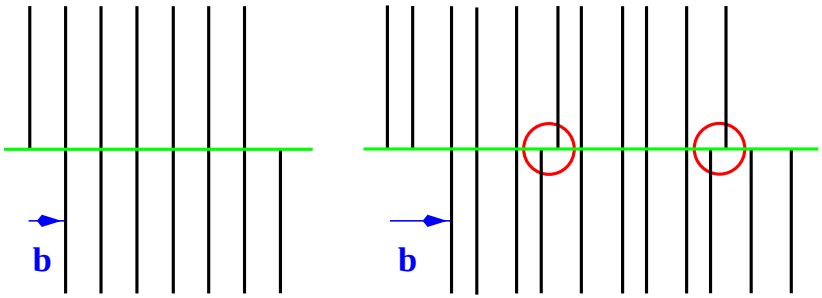

Figure 2.10: *Schematic representation of plastic deformation in a periodic and quasiperiodic sequence of planes.*

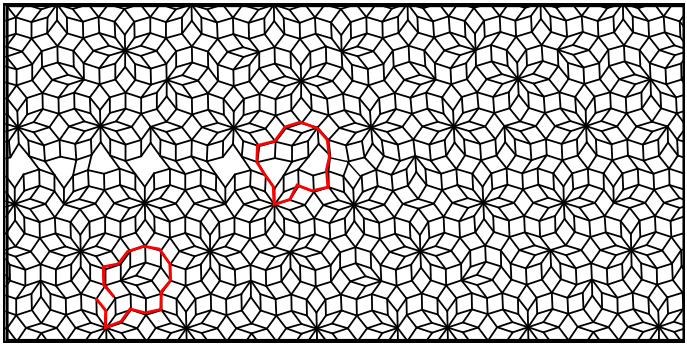

Figure 2.11: *Dislocation in a two-dimensional tiling. The position of the dislocation is indicated by the Burgers circuit.*

a perfect match of the two regions. In the quasiperiodic structure the planes are arranged in a sequence of long and short distances according to a Fibonacci sequence. Due to the quasiperiodicity of the sequence it is not possible to shift the upper part such as to bring the two halves in registry. As a consequence such a shift always results in a stacking-fault-like plane defect with mismatches indicted by the red circles.

In quasicrystals plastic deformation is mediated by motion of dislocations [45]. In perfect analogy to periodic crystals, dislocations in quasicrystals are line defects that are characterized by their line direction and their Burgers vectors [46]. In perodic lattices the Burgers vector can be estimated by performing a Burgers circuit around the dislocation. As mentioned above in quasiperiodic lattices the vertices can be uniquely written as an integer linear combination of basis vectors. Thus the Burgers vector in a quasiperiodic lattice can be defined in the same way as in periodic lattices.

Fig. 2.11 shows a dislocation in a two-dimensional binary tiling obtained by connecting nearest neighbours of different types. The position of the dislocation is indicated by the Burgers circuit. The dislocation leaves in its wake a plane defect which gives rise to differences in the atomic environments compared to the perfect quasicrystal.

Quasiperiodic tilings can be obtained by projection from a higher dimensional hyper-lattice. Thus the Burgers vector carries components $b^{\parallel}$ the physical space and components $b^{\perp}$ in the orthogonal space. The stacking fault separates two areas with a phase difference $b^{\perp}$ and is therefore called a phason wall [47]. As we will see later on the properties of the phason walls play an important role in crack propagation in quasicrystals.

Chapter 3

Fracture Mechanics

Fracture is the catastrophic failure of a solid due to external or internal loads. Fracture can occur in many different ways including fast crack propagation, stress corrosion cracking, hydrogen embrittlement, fatigue or creep. In the fracture process a large variety of phenomena is involved that occur on many different scale-levels, ranging from the atomic scale where cohesive bonds rupture to the macroscopic scale where devices break into part. Moreover, the modes of fracture do not only depend on the properties of a solid but also on the way the external load is applied or the conditions of the environment.

In the simplest classification scheme materials are divided into brittle materials if they shatter like glass and ductile if they are deformable. Whereas perfectly brittle materials fail without significant plasticity, ductile failure is associated with large plastic deformations.

In most cases the catastrophic fracture is a consequence of the unstable propagation of a crack from a pre-existing defect. Thus the starting point for investigations of fracture phenomena is the study of single crack propagation. The discipline of fracture mechanics has been created to explain such phenomena. Although fracture mechanics is a rather young discipline in materials science there exist a large variety of different models and concepts (for reviews see [48,49,50,51]).We restrict ourselves to the most important results that are relevant for the current work.

3.1 Linear Elastic Fracture Mechanics

Linear elastic fracture mechanics is treating cracks as free internal plane surfaces of an elastic continuum. Although realistic cracks have a three-dimensional character the stress and strain fields are treated as two-dimensional fields by assuming the crack front to be a straight line to make the problem mathematically handable.

Irwin observed that the motion of a crack can be divided into the three different propagation modes shown in Fig. 3.1. The modes are termed

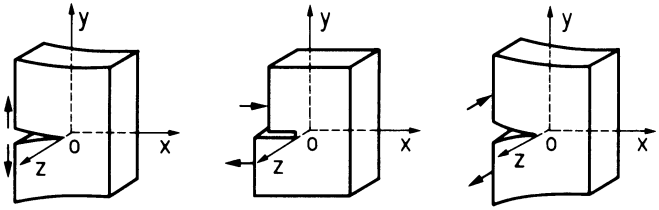

Figure 3.1: *The three modes of crack loading (I) opening, (II) sliding and (III) tearing mode.*

as opening, sliding and tearing mode according to the motion of the upper and lower crack surface with respect to each other.

The probably most important result of linear elastic fracture mechanics is that the stress fields carry a singularity at the crack tip that decays as the inverse square root of the distance R from the crack tip. For a semi-infinite crack in an infinite plate the relevant compounds of the stress field around the crack tip can be expressed as a linear combination of the three pure modes (see for example [50]):

$$\sigma_{ij} = \sum_{\alpha=1}^{3} K_\alpha \frac{1}{\sqrt{2\pi R}} f_{ij}^{\alpha}(\theta) \ , \tag{3.1}$$

where f_{ij}^{α} are functions of the angle θ between $\mathbf{R}$ and the crack plane. The strength of the singularity is characterized by the stress intensity factors K_α for mode α loading (I = opening, II = in-plane shear, III = out-of-plane shear). Although the geometry of the specimen and its macroscopic dimension determine the stress concentration at the crack tip, the occurrence of the square root singularity is independent of the particular loading conditions.

3.2 Fracture Criteria

The linear elastic continuum description allows to calculate the values of the stress field but it does not answer the question, under which conditions a crack will propagate. An explicit fracture criterion to predict crack propagation is the Griffith criterion. It can be formulated as a balance of the crack driving force, the energy release rate G, and the surface energy 2γ of the two freshly exposed fracture surfaces: $G = 2\gamma$. For pure mode I loading G is related to the stress intensity factor by $G = K_I^2/E'$, where E' is an appropriate elastic modulus [50]. This criterion implies the assumption of thermodynamic equilibrium for the crack tip. Since crack propagation is clearly a non-equilibrium phenomenon, the Griffith criterion constitutes only a necessary condition for crack propagation. It does not explain in which direction the crack will propagate [30].

As mentioned above, materials are classified as brittle if they shatter like glass and ductile if they are deformable. Whether a crystalline material is intrinsically brittle or ductile depends on its ability to emit dislocations from the crack tip. Once a dislocation has nucleated, its stress field can shield the forces acting on the crack tip and prevent the crack from moving. In addition, the driving force on the crack tip is lowered because the dislocation can blunt the crack tip. Thus cleavage and dislocation emission can be seen as competing processes for the failure of crystals. A simple criterion to decide whether a crystal is brittle or ductile was proposed by Rice and Thomson [52]. It is based on the calculation of the forces that act on a fully formed dislocation in the presence of a sharp crack. This force turns out to be attractive for small distances r but becomes repulsive for large values of r. The crack is considered as stable against emission of a blunting dislocation when the equilibrium distance r_0 is small, compared to a characteristic length, the so-called core cut-off radius of the blunting dislocation.

More sophisticated methods that consider the atomic structure of the blunting dislocation use the Peierls concept in the analysis of dislocation formation at the crack tip [53, 54]. The resistance of the crack to dislocation nucleation is then approximately characterized by the so-called unstable stacking fault energy γ_{us}. It represents the energy barrier that has to be overcome for a dislocation to nucleate from the crack tip.

Ductile failure is also favored, if other dislocation sources near the crack tip allow nucleation of new dislocations. This usually occurs at much lower stresses than predicted by the Peierls model. In either case, once nucleated the dislocation has to be able to move away from the crack tip to build a reasonably sized plastic zone. The latter requires sufficient dislocation mobility, which is the reason why the brittle or ductile response also depends on temperature and loading rate [55]. Whereas for crystals there exist different models for the brittle to ductile transition, it is less well understood in amorphous or quasicrystalline materials [56]. Essentially, the concepts are all based on the periodicity of the underlying structures and do not directly apply to quasicrystals. In the current work we study the influence of dislocation nucleation on crack propagation of model quasicrystals.

The continuum description poses two major problems. First, the stress singularity leads to infinite stresses at the crack tip. Thus in its vicinity the linear elastic continuum description loses validity. Second, the atomistic character of the material is not taken into account. Whereas the first problem can be overcome by surrounding the crack with a non-linear region, the discrete nature of solids can hardly be modeled by theories that are based on continuum considerations. Although the anisotropic linear elastic continuum analysis of a sharp crack tip [50] considers the crystallographic orientation of the crack system via appropriate elastic constants it is not able to describe phenomena that arise from the discrete structure of solids.

3.3 Cracks in Discrete Structures

An example how the atomistic structure influences crack propagation is the so-called lattice trapping effect [57]. Models of fracture that are based on continuum considerations like the Griffith theory predict that a crack is stable for unique stress level. For larger stresses the crack extends, whereas for lower stress levels it recedes. From an atomistic point of view cracks propagate by the breaking of bonds at the crack tip. Thus the resistance of a crack to propagate should be characterized by the forces that are needed to separate atomic bonds at the crack tip.

Early atomistic studies of fracture showed that cracks may be stable and do not advance until loads are applied that are somewhat larger than the Griffith value [57]. This effect was termed lattice trapping because the crack is "trapped" by the lattice. The lattice trapping can be viewed as the equivalent of the Peierls barrier, which impedes the motion of a dislocation. Detailed atomistic studies show that the effect depends strongly on the interatomic potential. It should be small for closely packed structures with soft interaction forces but should be more pronounced for open structures that are modeled by stiff potentials [58, 59].

From continuum considerations it is not expected that the fracture process depends on the direction of propagation on one cleavage plane. However, a pronounced anisotropy is observed experimentally for both single crystalline metals [60] and semi-conductors [61, 62]. This can also be explained by the lattice trapping effect. The magnitude of the trapping depends on the detailed arrangement of the bonds at the crack tip. Thus the barrier for the crack to advance can vary significantly for different orientations of the crack front on the same fracture plane [30].

Other examples of the influence of the lattice trapping effect on the fracture process, including the occurrence of metastable fracture planes, and thermal activated cleavage are given in [30].

Chapter 4

Crack Propagation and Molecular Dynamics

In the current work crack propagation is studied by using molecular dynamics simulations. In molecular dynamics simulations the trajectories of a set of particles are calculated by integrating numerically Hamilton's equations of motion for the multi particle system.

In this chapter we will focus on topics of molecular dynamics simulations that are related to simulations of crack propagation and particularly to simulations at finite temperatures. A detailed introduction into general concepts of molecular dynamics is given in [63].

Molecular dynamics simulations have proven a powerful tool in the study of crack propagation on the atomic scale [64,65,66,67,68,69,61,70,71,72]. While the first fracture simulations were performed with several hundreds of atoms [73], today simulations with a billion atoms are possible on massive parallel computers [74].

MD is particularly attractive for fracture studies because it allows to study crack propagation on the atomic scale. In continuum theories an explicit fracture criterion is needed to predict under which conditions a crack will propagate. In molecular dynamics a stable crack can be driven into the mechanical instability by application of an external load.

In contrast to periodic crystals, in quasicrystals there exist a large variety of atomic surroundings. Although quasicrystals are homogeneous on the macroscopic scale and in most cases densely packed structures, they contain clusters which are assumed to play an important role for their mechanical properties. MD allows to follow the trajectory of each atom in the simulation cell. Thus it is particularly suitable to study the influence of such intrinsic structure elements.

The simulations were performd by using the IMD (ITAP Molecular Dynamics) [75,76,77,78] package which was originally developed to study mechanical properties of quasicrystals. IMD was used for studies of crack propagation [3] and motion of dislocations [79,80] in quasicrystals

and for simulations of mechanical properties in covalent and metallic systems [81].

4.1 Interaction Potentials

To study crack propagation by molecular dynamics [63] one has to choose a structure model and a suitable model for the atomic interactions. Since the atomistic model can only answer questions that are within its validity, it is crucial to take great care in selecting a suitable interaction. For metals and covalent systems there exists a wide range of semi-empirical material specific potentials that mimic real materials. For most quasicrystals realistic interactions and structure models are not available at the moment. Although there are semi-empirical pair potentials for decagonal quasicrystals, these are pure bulk potentials. They do not even stabilise a free surface. Reliable potentials for crack propagation are not available. Therefore a generic pair potential is chosen to model the atomic interactions, and we do not make the attempt to mimic one particular material.

4.2 Boundary Conditions

In the framework of linear elastic continuum mechanics crack propagation poses a pure boundary value problem. However, analytical solutions for finite bodies with boundaries other than crack faces are rare. Most of the results are approximate in character and obtained under the assumption of small-scale yielding [82]. This is the situation that arises when the region around the crack tip, where plastic or inelastic deformations occur, is small compared to the length of the crack and the other dimensions of the body. In this case the stresses in the linear region near the crack tip but far away from the boundaries of the body are well described by the stress intensity factor. This means that the stress field of the crack is characterized by a weak $1/\sqrt{R}$-singularity. For molecular dynamic studies, where only a finite number of atoms can be treated, this long range character of the stress field has to be considered via appropriate boundary conditions. One possibility is to choose a large sam-

ple where the border atoms of the sample are held fixed and the atoms are displaced according to the linear elastic solution of a semi-infinite stable crack. The crack tip region is then relaxed to find the minimum energy configuration. Subsequently the system is driven into a mechanical instability by gradually increasing the strain on the borders until the crack propagates. These boundary conditions are particularly appropriate for simulations where material-specific interactions allow to calculate the load at which the instability of the mechanical system occurs.

They are not suitable, however, for our simulations for the following reasons: i) Even small changes at the crack tip have an influence on regions far away from the tip. Once the mechanical instability is reached and the crack starts to propagate the changes of the atomic positions at the crack will be carried far away due to the long range character of the crack field. One therefore has to make the sample very large so that the changes at the crack tip are negligible for the fixed atoms at the boundary. ii) They require to specify the location of the crack tip. The way the crack propagates is expected to depend on the local atomic arrangement in the vicinity of the crack tip. In quasicrystals there exists a large variety of different atomic surroundings. Thus the crack propagation can vary for different positions of the crack tip.

The boundary conditions should meet the following requirements: i) The crack should be able to experience the large variety of local atomic surroundings. ii) They should allow for an accurate control of the energy that is transferred to the crack tip. These requirements can be fulfilled by using a strip geometry that allows to study crack propagation with constant energy release rate. We explain the boundary conditions for the two-dimensional case. The extension to three dimensions is straight forward and is done by applying periodic boundary conditions along the crack front. Consider a thin strip of finite width containing a crack that reaches from one short side to one third of the strip length. By making the strip very long one can achieve that far ahead of the crack tip the strip is homogeneously strained. In contrast, at the pre-cracked side far behind the tip the crack surfaces are fully relaxed. The crack advance can be viewed as replacing a strip of material that is homogeneously strained by a strip with two fully relaxed surfaces. The energy difference is of course independent of the crack tip position and the crack thus

propagates with a constant energy release rate and at a constant driving force irrespective of its position in the strip.

Although these boundary conditions allow to control the energy that flows out through the crack tip very accurately, it has some drawbacks. The major drawback is that due to the finite number of atoms that can be treated the strip has to be of finite width. This implicates that the stress field is confined to the region between the fixed boundaries. Thus one would like to make the short length of the crack very large to take the long range character of the stress field into account. However, to follow the crack over a sufficient long time one would like to make the strip as long as possible. The aspect ratio has to be chosen to be appropriate for the problem under investigation. The aspect ratio was chosen to be 3.5.

It turns out that the limiting factor for the length of the strip is not given by the elastic properties of the sample but is due to the waves that are emanating from the crack due to the breaking of bonds at the crack tip.

4.3 Stabilising and Loading of Cracks

For zero temperature the crack is introduced by applying an approximate displacement field followed by a relaxation. For this purpose the strip is initially strained perpendicularly to its long axes to the Griffith load where the energy release rate G is equal to the surface energy of the two crack surfaces 2γ. Then the atoms are displaced perpendicular to the long axes of the strip so that the resulting crack is of elliptical shape. The system is relaxed by using an overdamped molecular dynamics scheme to obtain the displacement field of the stable crack at zero temperature. Subsequently the crack can be loaded by scaling all atomic displacements relative to the positions in reference system without crack. Such scaling of the atomic displacements does not change the overall shape of the elastic strain field [69]. This allows to change the load level in a very smooth way without creating any shock waves or otherwise disturbing the crack field.

The procedure is, however, not appropriate for finite temperatures. The first problem is to stabilize a crack. At finite temperatures there is no relaxation scheme that ensures to find a configuration of minimal *free*

energy. It is obvious that a displacement field that obeys the boundary conditions is (as for zero temperature) not available in analytical form. Nevertheless, an approximation can be obtained by using the zero temperature displacement field.

The second problem is how to load a crack at finite temperatures. For zero temperature the crack is loaded by linear scaling of the displacement field. The displacement field can be easily obtained by subtracting the atomic positions in a configuration containing a stable crack by its position in a reference system (without a crack). This procedure is inappropriate for finite temperatures due to the thermal fluctuations. By subtracting two configurations one obtains a displacement field that is disturbed by thermal fluctuations. Thus, linear scaling of the displacement field would result in a scaling of these perturbations. This effect is presumably small for low temperatures and narrow loads. Nevertheless, for elevated temperatures and large loads it may change the results significantly. The basic idea is to use an averaged displacement field obtained by taking the time average so that the thermal fluctuations are canceled out.

The position of an atom i at time t in the configuration containing a stable crack at temperature T can be written as

$$\mathbf{x}_i(t) = < \mathbf{x}_i >_T + < \mathbf{u}_i >_T + \Delta\mathbf{x}_i(t), \tag{4.1}$$

where $< \cdot >_T$ denotes the time average at temperature T. The position consists of the average position $< \mathbf{x}_i >_T$ in the reference system without crack, the average displacement field of the stable crack $< \mathbf{u}_i >_T$, and the deviation from the average position $\Delta\mathbf{x}_i(t)$ that arises from the thermal motion.

To stabilise the crack at a finite temperature T we start by approximating $< \mathbf{u}_i >_T$ by the displacement field for zero temperature. For this purpose we scale $< \mathbf{u}_i >_{T=0}$ by a factor $\alpha^*(T)$. This factor depends on the thermal expansion of the system $\alpha(T)$, the elastic constants and the surface energy. To estimate the value of $\alpha^*(T)$ for different temperatures one, in principle, has to know the temperature dependence of these values. However, we are not interested in the exact value of $\alpha^*(T)$ since it provides only a value for an approximated displacement field.

Figure 4.1: *Sketch of the simulation geometry for the simulations with stadium damping. The strength of the damping factor is indicated by a grey scale.*

In particular for quasicrystals where the critical load is expected to depend strongly on the local arrangements of atoms around the crack tip this value is of minor interest. Thus, we increase the value, beginning from the thermal expansion of the system until we get a stable crack for the respective temperature.

Once the crack is stabilised at a given temperature T the single contributions in (4.1) are easily accessible. By averaging over the atomic positions for several thousand time steps we can eliminate the thermal motion of the atoms to obtain the time-independent part of (4.1): $< \mathbf{x}_i >_T + < \mathbf{u}_i >_T$. By averaging over the reference system without a crack we can calculate the average positions $< \mathbf{x}_i >_T$. The average displacement field $< \mathbf{u}_i >_T$ is now obtained by subtracting these two values for each atom. The stable crack is subsequently loaded be adding a fraction of the displacement field to the positions of the stable crack configuration. The overloads are given by ΔK^* in the following, which is the relative fraction of the stress intensity factor due to the displacement field that is added to the stable crack.

4.4 Molecular Dynamics with Stadium Damping

There exists a large variety of methods to perform molecular dynamics simulations at finite temperatures (for review, see [63]). The probably most popular among these is the so-called Nosé-Hoover thermostat [83, 84, 85]. It is often used for *equilibrium* molecular dynamics studies, because it allows to calculate thermodynamic averages via estimating simple statistical averages. The equations of motion are extended by adding a 'friction coefficient' to the equations of motion:

$$\dot{\mathbf{r}} = \frac{\mathbf{p}}{m} \tag{4.2}$$

$$\dot{\mathbf{p}} = \mathbf{F} - \xi \mathbf{p} \tag{4.3}$$

The time-evolution of the friction coefficient ξ is given by the first-order differential equation $\dot{\xi} = N(k_B T - k_B T_0)/Q$, where N is the number of degrees of freedom in the system, T_0 is the desired temperature, and Q is the thermal inertia parameter which is a constant. The value of Q is chosen to be equal to the inverse of the characteristic vibrational frequency of the system [86]. The instantaneous temperature T is calculated by averaging the atomic velocities for all atoms in the system. Since crack propagation is essentially a non-equilibrium process, where a large amount of energy is dissipiated from a narrow region at the crack tip, the Nosé-Hoover thermostat is inappropriate for such simulations.

The crack advance is connected to the breaking of atomic bonds at the crack tip. This results in acoustic waves that are emitted from the crack tip. To study crack propagation by means of molecular dynamics one has to study systems of finite size. The load is applied through the boundaries where the atoms are held fixed during the whole simulation. Waves that are reflected from the boundaries of the system can even result in a crack arrest as was shown by Holian and Ravelo [65]. Thus the integration scheme should not only allow to maintain the temperature of the system, but it should also prevent that waves which are emitted from the crack tip are reflected by the fixed boundaries.

The method that is applied here was proposed by Holian and Ravelo [65]. It is a modified version of the thermostat introduced by Berendsen *et*

al. [87]. Acoustic waves emanating from the crack tip are absorbed by ramping up a viscous damping in a region around the crack tip. For this purpose an elliptical stadium function f is used with

$$f(\mathbf{r}) \quad = \quad \min\left[1, \max\left(0, \frac{(x/L_x)^2 + (y/L_y)^2 - (a/L_x)^2}{1/4 - (a/L_x)^2}\right)\right] \tag{4.4}$$

where L_x and L_y are the long and short half length of the strip. The damping coefficient is zero in an elliptical region with a long half axes of length a. The equations of motion are

$$\dot{\mathbf{r}} \quad = \quad \frac{\mathbf{p}}{m} \tag{4.5}$$

$$\dot{\mathbf{p}} \quad = \quad \mathbf{F} - \gamma \; f \; \mathbf{p}. \tag{4.6}$$

In contrast to the Nosé-Hoover thermostat the strength of the damping is not given by a first-order differential equation but is calculated as

$$\gamma \quad = \quad \bar{\gamma}\left(1 - \frac{T_0}{T}\right) \tag{4.7}$$

where T_0 is the desired temperature and the instantaneous temperature T is calculated by a weighted sum over the momenta of the particles

$$kT \quad = \quad \frac{\sum f \; \mathbf{p}^2/m}{2 \; \sum f}. \tag{4.8}$$

The damping pre-factor $\bar{\gamma}$ is taken to be twice the Einstein frequency ω_E which has been shown [65] to efficiently absorb outgoing elastic waves of almost all frequencies.

In the previous section the scaling procedure to load the crack was only applied to the atomic positions. To get an initial condition at finite temperatures one also has to specify the atomic velocities. However, the velocity distribution for the stable crack is unknown. As mentioned above, the center of the stadium is free of any viscous damping. In the viscous damping region the temperature is maintained, whereas in the center region, where Newtonian mechanics applies, the total energy is conserved. Application of an unappropriate velocity distribution may thus lead to a temperature gradient between the two regions which is

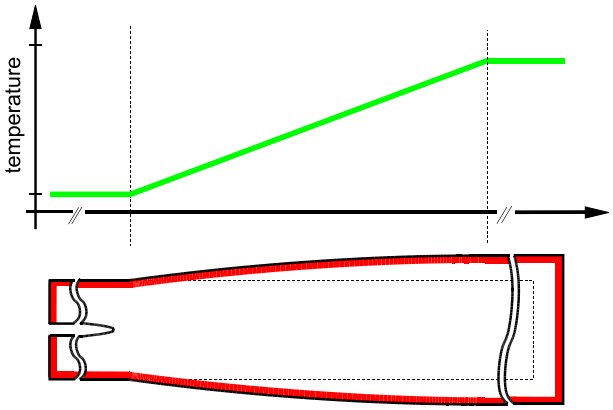

Figure 4.2: *Sketch of the simulation geometry for the simulations with temperature gradient.*

obviously unwanted. After adding a displacement field we start by applying the viscous damping over the whole system by setting the damping pre-factor f to unity for the whole strip. Subsequently f is reduced until the distribution of equation (4.4) is reached.

4.5 Crack Propagation with Temperature Gradient

To stabilise the crack at different temperatures one can use the procedure described above and scale the displacement field to a given temperature by using the thermal expansion of the system. In principle it is possible to reach any temperature by scaling the crack successively from low temperatures to high temperatures. However, it should be noted that this approach works only as long as the crack remains atomically sharp. To obtain the displacement field one has to average over sufficiently long time intervals that the thermal motions are cancelled out. Obviously this is not possible when the crack tip deforms irreversibly, e. g. dislocation nucleation. In our simulations we observe that for temperatures above $30\%\, T_m$ the crack does not remain atomically sharp

but blunts spontaneously. Thus, it is not possible to average over a sufficiently large number of time steps to obtain a stable initial condition for a sharp crack.

To overcome this problem and to nevertheless study brittle crack propagation at higher temperatures we introduce a new simulation geometry which mimics an experimental setup which is used to study the brittle to ductile transition [88, 89]. In these experiments a crack is driven up a temperature gradient from a cold region where it propagates by brittle cleavage to a high temperature region, where it suddenly arrests. By measuring the temperature gradient along the sample, the brittle to ductile transition temperature for a given loading rate can be determined from the position of the crack arrest.

We use a very long strip with an aspect ratio of 10. A linear temperature gradient is applied along the strip and the crack is introduced on the low temperature side where a sharp tip can be stabilized. The crack is then driven into a region of elevated temperature by loading the sample as described in the previous section.

To establish the temperature gradient along the strip we use a local temperature control scheme [90, 69], which resembles an electronic heat bath for the ions. The equations of motion for atom i are given by

$$\dot{\mathbf{r}}_i = \frac{\mathbf{p}_i}{m_i} \tag{4.9}$$

$$\dot{\mathbf{p}}_i = \mathbf{F}_i - \gamma_i \, \mathbf{p}_i. \tag{4.10}$$

The damping factor γ is calculated from

$$\gamma_i = \bar{\gamma}_0 \, \frac{T_i - T_0}{\left[T_i^2 + (T_0/\delta T)^2 \right]^{1/2}}, \tag{4.11}$$

where T_0 is the desired temperature at the position of particle i and T_i is its kinetic temperature. The factor $\delta T = 20$ is used to keep γ_i finite for atoms at rest and has been chosen to be compatible with the time step. $\bar{\gamma}_0$ represents the strength of the heat bath and is a constant of the order of unity.

Corresponding to the applied temperature gradient, the system is expanded to balance the thermal expansion, which results in a telescope shape of the specimen (Fig. 4.2).

Chapter 5

Crack Propagation in Decagonal (2D) Quasicrystals

5.1 Decagonal Binary Model Quasicrystals

The Mikulla-Roth tiling (MRT) introduced in Section 2.5.1 shares central properties with structure models for real quasicrystals, namely a quasiperiodic plane structure and a hierarchical structure of decagonal clusters. The smallest clusters are given by concentric rings of ten small and ten large atoms (Fig. 5.2), and can be considered as two-dimensional versions of Mackay or Bergman clusters which are significant for real quasicrystals. The clusters themselves are arranged on families of parallel planes (Fig. 5.1). The planes occur with two different distances, according to a Fibonacci sequence. Due to the decagonal symmetry of the system, equivalent families of lines result from rotations by 36°.

The random tiling model is constructed from a perfectly ordered MRT by increasing the phason degree of disorder through random phason flips [91]. The symmetry of the resulting random tiling is still decagonal as for the MRT but the frequencies of the atomic surroundings are different. The tenfold clusters of the MRT are mostly destroyed.

Fig. 5.1 shows the two model quasicrystals in two different representations. In the atomic representation the two species of atoms are represented as discs. The bond representation is obtained by connecting nearest neighbors of different type. Defects in quasicrystals are always associated with the occurrence of forbidden local surroundings. Thus the bond representation is particularly suitable to display dislocations and phason walls.

The atomic interactions are modeled by Lennard-Jones (LJ) potentials [92], originally derived for the van der Waals-type interaction of inert gases. For the binary systems one has to specify potentials for the AA, BB, and AB interactions, respectively (see Fig. 5.3).

Both model quasicrystals, the MRT and the random tiling system are decagonal binary tilings (BT). In BT the bond length fulfill the require-

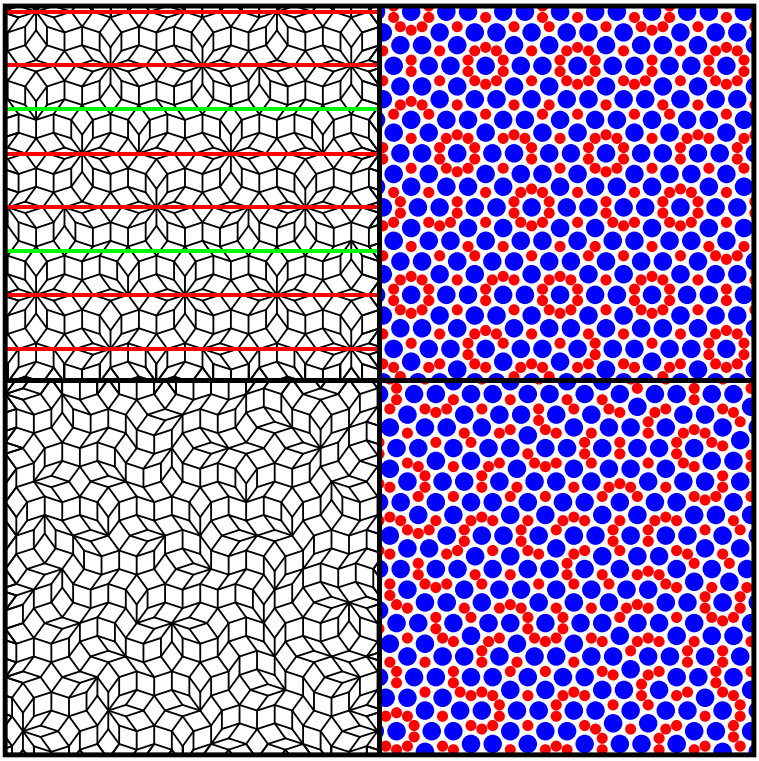

Figure 5.1: *The binary model quasicrystals: MRT (top) and random tiling (bottom). Left: Bond representation obtained by connecting nearest neighbors of different types. Right: Atomic representation where the two species of atoms are represented as discs. Planes with low surface energy are indicated by light lines.*

ment that five particles of type A surround one B particle and ten B particles surround one A particle. The bond lengths are chosen to be the geometrical ones. The depths of the LJ potentials are ϵ_0 for AA and BB bonds and $2\epsilon_0$ for AB bonds. With this choice of parameters for the LJ potentials the highest coordinated decagonal clusters become the tightest bound structural units of the quasicrystal. The unit of length r_0 is

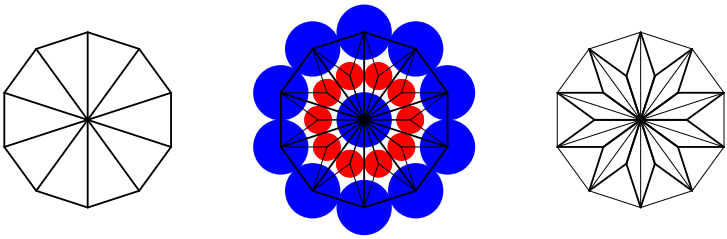

Figure 5.2: *Ten-rings in atom (middle) and bond representation (right) and origin in the triangle tiling (left).*

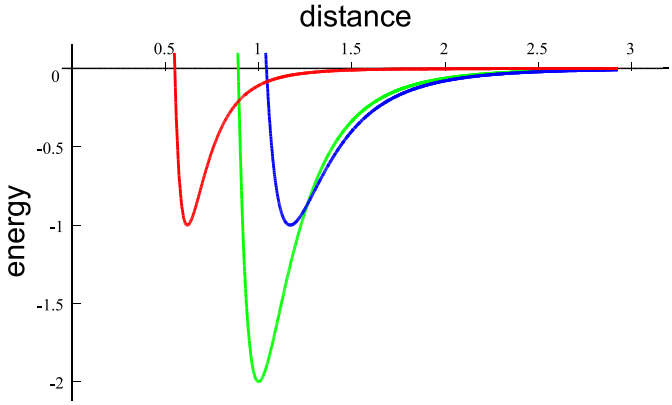

Figure 5.3: *Lennard–Jones–Potentials for the three interactions. The depth of the potentials are ϵ_0 for AA and BB bonds and $2\epsilon_0$ for AB bonds.*

the same for all three interactions and corresponds to the length of one AB bond in the structure. For computational efficiency a finite-range cutoff was imposed on all potentials by setting them equal to zero for separation distances greater than $2.925r_0$. All masses are set to unity and the time is measured in units of $t_0 = r_0\sqrt{m/\epsilon_0}$.

5.1.1 Thermal Stability

For fixed stoichiometry all binary tilings have same energy for pair-wise interactions that are restricted to first neighbors [93]. Indeed the model in this work has a crystalline ground state [94]. However, the model quasicrystals are thermally stable at least for the time scales accessible for molecular dynamics simulations [95].

To calculate the melting temperature for both systems we use a periodic approximant containing approximately 30.000 atoms. The simulations were carried out by using a Nosé-Hoover thermostat [96, 97, 98] and the pressure is maintained using an Anderson barostat [99]. The system was heated by increasing the temperature linearly from a temperature of about 10% of the melting temperature $0.1\epsilon_0$ until the system was melted. The melting transition was detected by monitoring the mean atomic volume Ω. At the melting temperature Ω undergoes a sudden upward jump. The melting temperatures are $0.64\epsilon_0$ for both systems.

The elastic constants were measured by deforming the same approximants homogeneously with periodic boundary conditions. For this purpose a linear fit to the stress-strain curves for both a simple shear deformation and uniform compression up to 0.5 %. The systems show an almost identical bulk modulus of 122.0 ϵ_0/r_0^2 and 122.3 ϵ_0/r_0^2 for the RMT and the random tiling respectively. The shear modulus μ was measured to be 50.6 ϵ_0/r_0^2 for the MRT and 52.6 ϵ_0/r_0^2 for the random tiling.

5.1.2 Visualization

Due to the large number of atoms required to study crack propagation, the reduction of data is of crucial importance. To study the dynamics of the crack one has to determine the position of the crack tip in quite short time intervals. It is not possible to always write out the positions of all atoms. Thus, one has to find criteria which allow to select only the atoms that carry the desired information.

In periodic crystals, defects can be visualized by plotting only those atoms whose potential energy exceeds a certain threshold [100]. In quasicrystals, however, atoms may have largely varying local environments. Their potential energy thus varies significantly from atom to atom, even

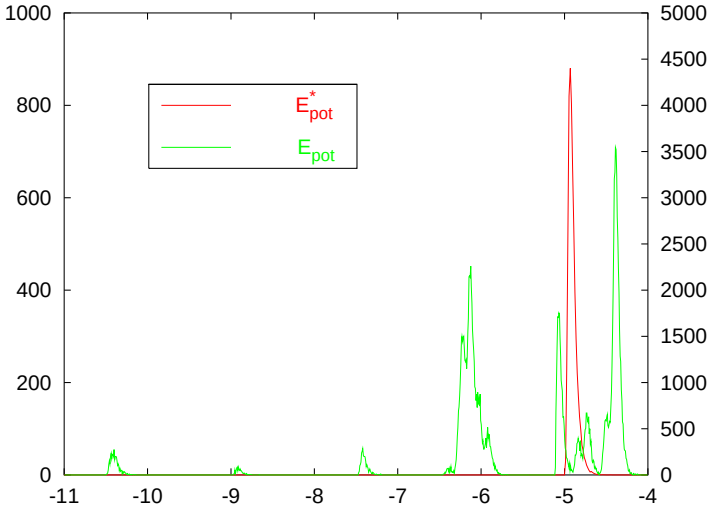

Figure 5.4: *Distribution of the potential energy E_{pot} and the weighted potential energy E^*_{pot} for a simulation at about $10\%T_m$.*

for atoms of the same type in a defect-free sample. Fig. 5.4 shows the distribution of the potential energy for a configuration at about $10\%T_m$. The distribution shows a broad spectrum of energies ranging from $-10.5\epsilon_0$ to about $-4\epsilon_0$. Defects can therefore not be visualized by applying a simple energy cut-off as in periodic systems. Nevertheless, a criterion can be obtained by using the specific properties of binary tilings.

For binary tilings the number of different atomic environments within the nearest neighbor distance is four and three for the large and small atoms respectively. Fig. 5.5 shows all possible nearest neighbor configurations that appear in a perfectly ordered MRT. The pair (n_S, n_L) denotes the number of small and large nearest neighbors. In the MRT n_S and n_L obey a linear relation that is $n_S/2 + n_L = 5$ for the large atoms and $n_S + n_L = 5$ for the small atoms.

By weighting the pair interaction $\varphi_{\alpha\beta}$ by the factors $\gamma_{\alpha\beta}$ it is possible to narrow the potential energy distribution. Fig. 5.4 shows the distribution

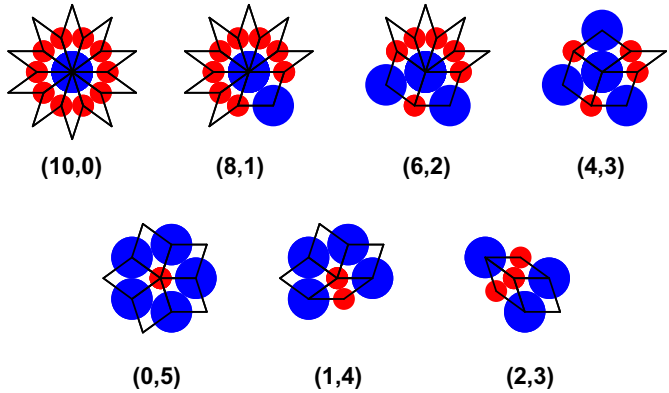

Figure 5.5: *Atomic configurations in the MRT where* (n_S, n_L) *denotes the numbers of neighbors of large and small neighbors.*

of the scaled potential energy for a configuration at about $10\%T_m$. The weights were chosen to be $\gamma^{LL} = 1/\epsilon_0, \gamma^{SL} = 1/(2\epsilon_0), \gamma^{LS} = 1/(4\epsilon_0)$ and $\gamma^{SS} = 1/\epsilon_0$. The distribution shows only one large peak with a width of about $0.2\epsilon_0$.

This makes it possible to detect defects like dislocations, phason walls and cracks by plotting only those atoms whose weighted potential energy exceeds a certain threshold.

5.1.3 Plane Structure

To stabilize a crack one has to specify an initial crack plane. According to the Griffith criterion, planes with low surface energy are potential fracture planes. For simple crystal structures like the face centered cubic structure of the noble metals the surface energy only depends on the crystallographic orientation of the surface. In quasicrystals, however, it even varies for crystallographically equivalent but structurally distinct surfaces.

To identify the planes of lowest surface energy we relax a specimen and split it in two regions. Subsequently, the two parts are shifted rigidly by a distance of $10r_0$ perpendicular to the cutting plane. The surface

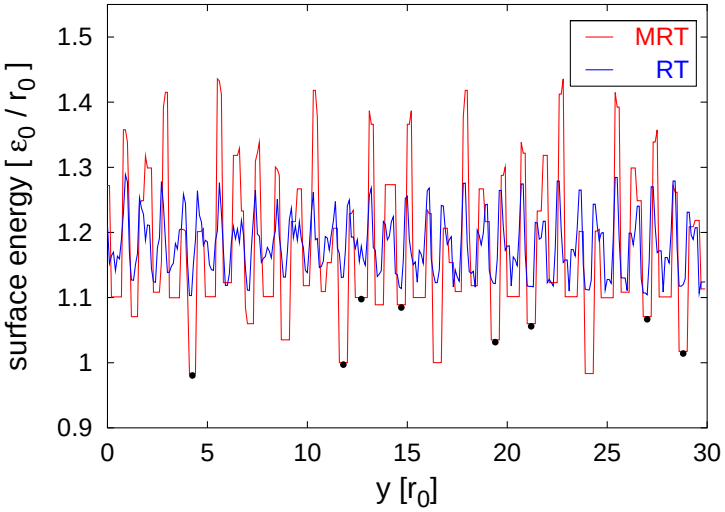

Figure 5.6: *Surface energy in dependence on the cutting plane. For the MRT the positions of the planes with lowest surface energy form a Fibonacci-sequence. The random tiling model shows no distinct plane structure.*

energy is then calculated from the difference in potential energy of the artificially cleaved and the undisturbed specimen.

It should be noted that this procedure does not allow to calculate the surface energy of a free surface. The difference between the artificially cut and the undisturbed system provides only a value for the *average* energy of the two generated surfaces. However, this is exactly the value that appears in the Griffith criterion. Thus, the term surface energy is used in the following.

Fig. 5.6 shows the surface energy for crystallographically equivalent surfaces as a function of the position of the cutting plane. In the MRT one finds a pronounced plane structure of low and high surface energies. The planes of lowest surface energy occur with two separations, arranged in a Fibonacci sequence. These correspond to the planes between the large

separation of the parallel lines connecting the clusters and are given by the light lines in Fig. 5.1.

The random tiling shows no such distinct plane structure. For the random tiling the difference between the planes of lowest and highest energy is only about $0.2\epsilon_0/r_0$ whereas for the MRT it is about $0.5\epsilon_0/r_0$. The surfaces of lowest energy is selected as initial fracture planes for the simulations in the MRT. The system is initially strained to the Griffith load where the energy release rate G equals to the surface energy of the two crack surfaces 2γ.

5.2 Low Temperature Propagation

In the low temperature regime of below $0.30\,T_m$ crack propagation was studied in both the perfectly ordered and the random tiling system in a strip geometry with stadium damping. Our samples consist of about 330,000 atoms in a strip of width $275\,r_0$ which corresponds to an aspect ratio of 3.5. All atoms in the outermost boundary layer of width $3\,r_0$ remain fixed during the simulation. The strip is homogeneously strained perpendicular to its long axis and an atomically sharp crack is inserted from one short side to one third of the strip length as described in Sec. 4.3. Crack propagation was simulated at three different temperatures that correspond to 10%, 20% and 30% of the melting temperature T_m.

5.2.1 Crack Tip Velocity

The samples are loaded by the procedure described in section 4.3. As mentioned above the loading procedure does not change the overall shape of the displacement field. As a result, the cracks reach their terminal velocity almost instantaneously.

To measure the crack tip velocity the position of the crack tip was inspected every 100 time steps. The crack tip position is plotted as a function of time. Subsequently the velocity is calculated from the slope of a linear fit to the position over time curve. Fig. 5.7 shows the ter-

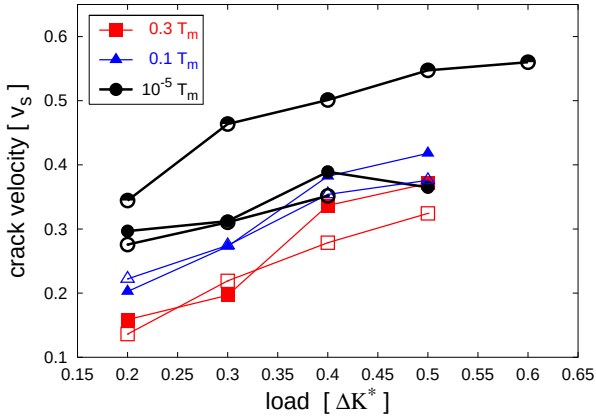

Figure 5.7: *Crack tip velocity in dependence on the load at various temperatures for the MRT with phason wall (half filled symbols) and without phason wall (filled symbols) and the random tiling model (open symbols).*

minal crack tip velocity as a function of the applied load for different temperatures.

For small loads up to $\Delta K^* = 0.2$ the crack propagates only a few atomic distances r_0 and then stops. The minimal velocity for brittle crack propagation is about 15% of the shear wave velocity v_s. The cracks are stopped by obstacles like incomplete tenfold clusters.

For loads in the range of $\Delta K^* = 0.30$ to 0.50 the crack velocity increases with the applied load just as in periodic crystals. However, the mode of propagation in the MRT differs significantly from that in periodic systems [101, 102, 6, 3].

5.2.2 Low Temperature Mechanism

The crack propagates on the initial fracture plane until it hits an obstacle. There a dislocation nucleates along a plane that is inclined by 36° (Fig. 5.8 a). The dislocation does not get farther away from the crack tip than $5r_0$ before it is blocked by another obstacle (Fig. 5.8 b). This

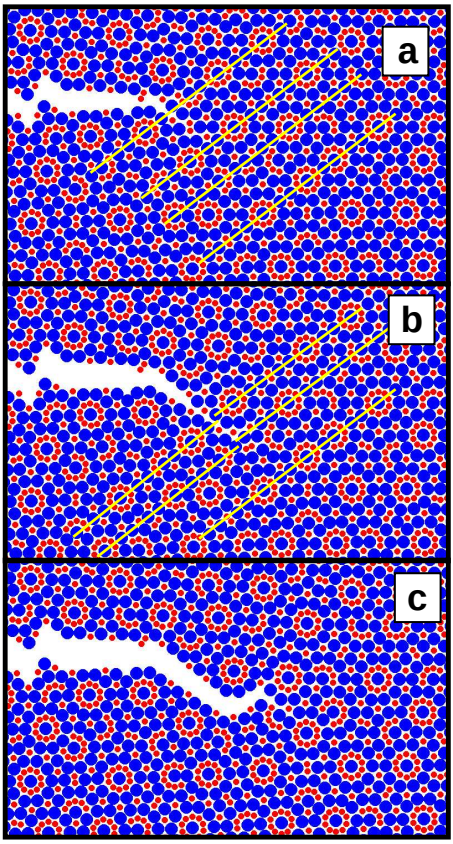

Figure 5.8: *Crack propagation mechanism in the MRT. (a) The crack propagates on the initial fracture plane. (b) It has emitted a dislocation that is followed by a phason wall. (c) The quasicrystal has opened up along the phason wall.*

is in agreement with simulations of dislocation mobility [27] which show that complete or incomplete clusters act as obstacles for moving dislocations. As mentioned above, the stress field of the dislocation is generally expected to shield the crack from the applied load which results in

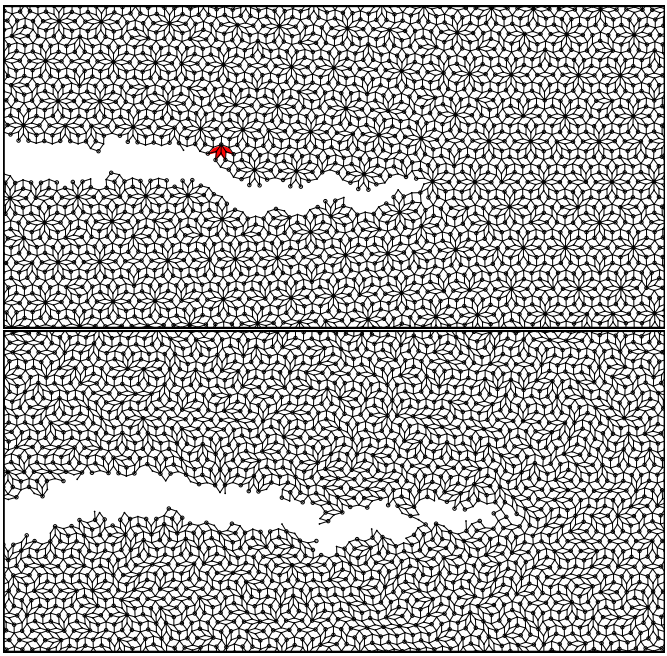

Figure 5.9: *Crack configurations from simulations at $T = 0.10T_m$ for the MRT (top) and the random tiling system.*

an increase of fracture toughness. Here, however, the crack follows the dislocation as can be seen in Fig. 5.8 c). This can be explained by the aperiodic structure of quasicrystals.

As mentioned before a moving dislocation in a quasicrystal leaves in its wake a plane defect that separates two areas with a phase difference $b^{\perp}$. This defect which gives rise to differences in the atomic environments compared to the perfect quasicrystal is called a phason wall [47].

Fig. 5.10 shows the disregistry energy [47], which is the potential energy necessary to shift one half of a quasicrystal rigidly over the other along a glide plane. For periodic crystals this energy is called γ-surface [103] and is a periodic, approximately sinusoidal curve with zero fault energy at multiples of the lattice vectors. For our model quasicrystal the dis-

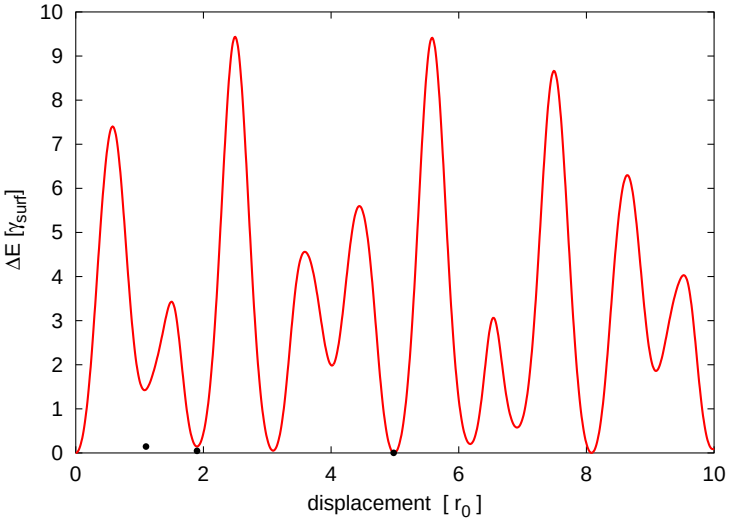

Figure 5.10: *Disregistry energy along a glide plane. The energy for the relaxed phason wall of the first minimum is about* 14% *of the surface energy.*

registry energy is quasiperiodic with two classes of local minima. Those of the first class are very deep with values of the order of 10^{-4} and represent the primary Burgers vectors of the model. The disregistry energy for the minima of the second class are of the order of 1. In contrast to periodic crystals, the disregistry energy in quasicrystals does not vanish but remains finite for any arbitrary choice of the displacement.[1]

The phason wall behind a dislocation emitted by the crack tip corresponds to the first minimum of the second class. The disregistry energy is in the order of the surface energy γ but is reduced by elastic relaxation to about 14% of γ. Thus along this wall the structure is weakened and the cohesive energy diminished, with the consequence that the material

[1] It should be noted here that the disregistry energy in our model quasicrystals can also vanish for large values of the Burgers vector due to the finite range of the interatomic potentials. The introduction of a phason wall results always in the occurrence of forbidden atomic surroundings. However, they do not affect the potential energy if the violations are not within the range of the interaction potential.

is preferably opening in this plane. The resulting fracture surface shows characteristic deviations of 36° to the initial fracture plane (see Fig. 5.9).

5.2.3 Influence of the Phason Wall

To confirm the low temperature propagation mechanism and to study particularly the influence of the phason wall on the propagation mechanism we construct artificial phason walls with different magnitude of Burgers vectors and simulate crack propagation along them. The walls are introduced by cutting the sample into halves along the fracture plane. Then the upper part is shifted rigidly for the length of the respective Burgers vector $b^{\parallel}$ in the direction parallel to the fracture plane. This yields a phason wall comparable to the one behind a dislocation with Burgers vector $b^{\parallel}$. Subsequently a crack is stabilized on the phason wall according to the procedure prescribed above. Fig.5.11 shows crack configurations from simulations along phason walls for different Burgers vectors.

We have chosen three different Burgers vectors with parallel components $b^{\parallel} = 1.1, 1.8$ and 4.9 respectively. The first value results in a high energy phason wall which corresponds to the first minima in Fig. 5.10. This phason wall is exactly the one observed in the fracture simulations. Dislocations with the same Burgers vector were also observed in shear simulations at low temperatures [104]. The phason wall for $b^{\parallel} = 1.8$ is the shortest primary Burgers vector for the first very deep minimum in Fig. 5.10 that carries a disregistry energy of about $10^{-3}\gamma$. Dislocations with the same Burgers vector were observed in high temperature deformation [95].

As mentioned before the phason wall separates two areas with a phase difference $b^{\perp}$, which gives rise to faults in the quasiperiodic pattern and therefore in the atomic environments compared to the perfect quasicrystal. The density of defects in a phason wall is monotonically but not linearly correlated with the absolute value of the perpendicular component $|b^{\perp}|$ of the respective Burgers vector.

There are two different types of phason defects. Those of the first type are given by the red nonconvex hexagons in Fig. 5.11 and appear along

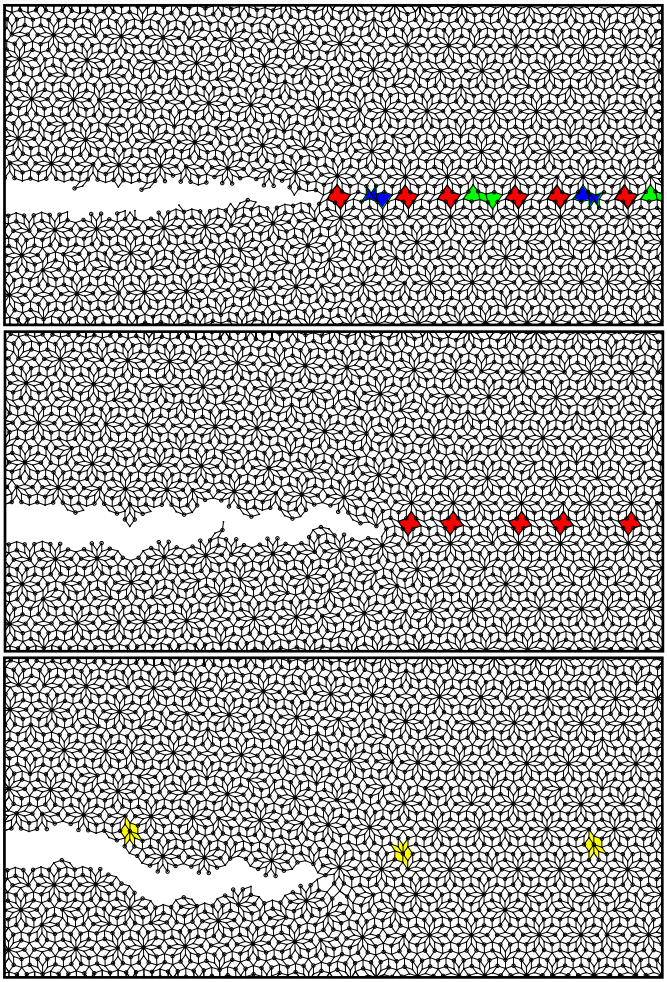

Figure 5.11: *Crack configurations from propagation along phason walls for Burgers vectors* $b^{\parallel} = 1.1, 1.8$ *and* 4.9 *(from top)*

the phason walls for $b^{\parallel} = 1.1$ and 1.8. This configuration is obtained by a single phason flip in the Tübingen triangle tiling. The resulting tiling

still consists of the two basic triangles. The configuration is "forbidden" for binary tilings, however, since it leads to tiles that differ from the two basic rhombi.

The defects of the second class are marked in blue and green in Fig. 5.11 and appear exclusively for high energy phason walls with Burgers vectors whose component $b^{\perp}$ are outside the acceptance domain [47]. In contrast to the defects of the first type they even result in voids in the Tübingen triangle tiling.

For the Burgers vectors $b^{\parallel} = 1.1$ the crack propagates without changing direction as can be seen in Fig.5.11 (top). As for the undisturbed quasicrystal the crack does not cut the tightly bound clusters. However, in contrast to the simulations without phason wall we do not observe the nucleation of dislocations from the crack tip. Thus the crack shows no deviations from the initial fracture plane which results in an extremely flat fracture surface.

The phason wall for Burgers vector $b^{\parallel} = 1.8$ contains only phason defects of the first type. Again the crack follows the phason wall without cutting the tightly bound clusters. However, the roughness of the resulting fracture surface is increased as can be seen from Fig. 5.11(middle).

The phason wall with $b^{\parallel} = 4.9$ does not contain configurations that lead to new tiles in the binary tiling. There exist local atomic configurations that do not appear in the undisturbed model quasicrystal. They consist of four thin and two fat rhombi and are highlighted in Fig. 5.11(bottom). In contrast to the situation for $b^{\parallel} = 1.1$ and 1.8 we observe nucleation of dislocations from the crack tip. The crack propagates on the initial fracture plane until it hits an obstacle which is given by an incomplete cluster. As a result the crack does not propagate along the phason wall but deviates from the initial fracture plane just like in the perfect quasicrystal.

The phason wall influences not only the morphology of the resulting crack planes but results also in a change in propagation velocity. Fig. 5.7 shows the crack tip velocity for propagation along the phason wall with $b^{\parallel} = 1.1$ over the applied load at $T = 10^{-5}T_m$. The crack tip velocity increases with the applied load just like in the perfect quasicrystal. However, the average crack tip velocity is increased by about 40%. A

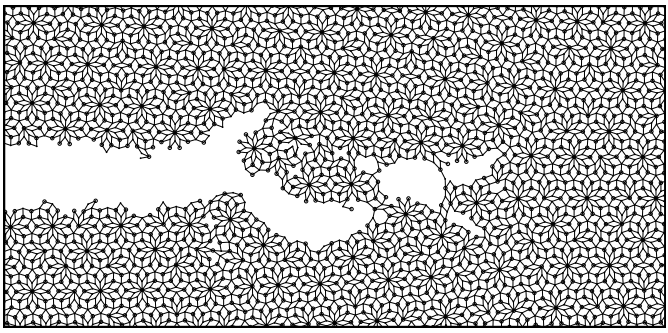

Figure 5.12: *Snapshot at* $\Delta K^* = 1.00$ *and* $T = 10\%\, T_m$. *The branches follow the easy planes that are inclined to the fracture plane by* $36°$.

similar increase in velocity is found for the phason wall with $b^{\parallel} = 1.8$. In contrast to this, for $b^{\parallel} = 4.9$ the crack tip velocity is comparable to that observed in perfect quasicrystals.

5.2.4 Crack Tip Instability

At loads above $\Delta K^* = 0.5$ the crack becomes unstable and branches. A typical configuration for the crack branching at $0.10\, T_m$ and a load of $\Delta K^* = 1.00$ is shown in Fig. 5.12. The branches form an angle of $72°$ and correspond again to the easy planes which are located at every $36°$ inclination from the fracture plane. The determination of a single crack tip position is obviously impossible. The crack velocity of the branches can roughly be estimated to lie in the range of $0.4 - 0.5\, v_s$.

Simulations of crack propagation in periodic crystals show that the crack tip speed increases with the applied load to a maximum value of about $40\% v_s$. Further increase of the load does not significantly change the terminal velocity [69]. This is explained by the nonlinearity of the atomic interaction which weakens in tension and strengthens in compression. As a result the coupling strength between the atoms behind the crack tip and the atoms at the tip is reduced. Thus the velocity at which information is transferred along the crack surface is reduced. This results in a lower terminal steady-state velocity compared to continuum analysis [69]. Such a behavior is also expected for our model quasicrystals.

However, in our simulations the velocity increases with the load until the crack bifurcates. We do not observe a plateau of constant velocity. For the propagation along the phason wall with $b^{\parallel} = 1.1$, the occurrence of the instability is shifted to higher loads of $\Delta K^* = 0.80$. Here we do observe an almost constant crack tip speed for loads between $\Delta K^* = 0.50$ and $\Delta K^* = 0.70$. Whereas the propagation along the phason wall resembles the behavior observed in periodic crystals the instability in the perfect quasicrystal occurs for smaller load levels and lower propagation velocities.

5.2.5 Random Tiling Quasicrystals

To study in detail which structure elements are responsible for the characteristic propagation mechanism in quasicrystals we study crack propagation in a random tiling system. The cracks are stabilized and loaded using the procedure described above.

The random tiling model is constructed from a perfectly ordered MRT by increasing the phason degree of disorder through random phason flips. The flips are rearrangments of tiles which leave the shape of the tiles unchanged. Thus the number of atoms and the stoichiometry is conserved. The symmetry of the resulting random tiling is still decagonal as for the MRT but the frequencies of the atomic surroundings are different. The tenfold clusters of the MRT are mostly destroyed. However, the number of incomplete clusters where two or more thin rhombi are placed around one large atom is increased (see Fig. 5.12).

As for the perfectly ordered system we observe brittle crack propagation. The dependence of the crack tip velocity on the applied load is very similar to that of the perfectly ordered system as can be seen from Fig. 5.7. However, the mode of propagation varies significantly from that in the MRT.

Dislocations in our model quasicrystal propagate exclusively on well defined crystallographic planes. By introducing the phason flips, the plane structure is destroyed. Thus the dislocation nucleation process is suppressed and the crack propagates by the breaking of single bonds. In contrast to the simulations in the MRT we do not observe the zig-zag

shape of the fracture surface. Crack configurations from simulations at $10\%T_m$ for the two systems are shown in Fig. 5.9.

For loads above $\Delta K^* = 0.5$ the crack becomes unstable as for the perfectly ordered system. In the MRT the branches follow the easy planes which are located at every 36° inclination from the fracture plane. Due to the lack of a pronounced plane structure the crack branches are less pronounced.

5.3 High Temperature Propagation

For the studies of crack propagation in the strip geometry with temperature gradient we use a very long strip of the same width as in the low temperature simulations. The sample consists of about 800,000 atoms with an aspect ratio of 10. A linear temperature gradient is applied along the strip and the crack is introduced on the low temperature side where a sharp tip can be stabilized. The crack is then driven into a region of elevated temperature (Fig. 4.2) by loading the sample as described above. Corresponding to the temperature gradient, the tip position can be directly translated into a temperature at the position of the crack tip (Fig. 4.2).

The crack is stabilized in a region with $T = 0.3\,T_m$ and the temperature is increased to $0.8\,T_m$ on a length of $1500\,r_0$. Acoustic waves emanating from the crack tip are absorbed by ramping up a viscous damping from a small finite value at the fracture plane to a maximum value at the outer boundary [69] as described in Sec.4.4.

For small overloads and shallow temperature gradients the crack stops in the medium temperature regime between $30-70\%T_m$ by spontaneous blunting of the crack tip. The crack travels at almost constant velocity until a dislocation nucleates along a plane that is inclined by 72° to the initial fracture plane. Fig. 5.14 shows the crack tip before and after nucleation of the blunting dislocation. The dislocation is framed by a Burgers circuit. Just like in the low temperature regime, the dislocation does not get farther away from the crack tip than $5r_0$ where it is blocked by an obstacle. This is in agreement with simulations of dislocation mobility [27] which show that complete or incomplete clusters

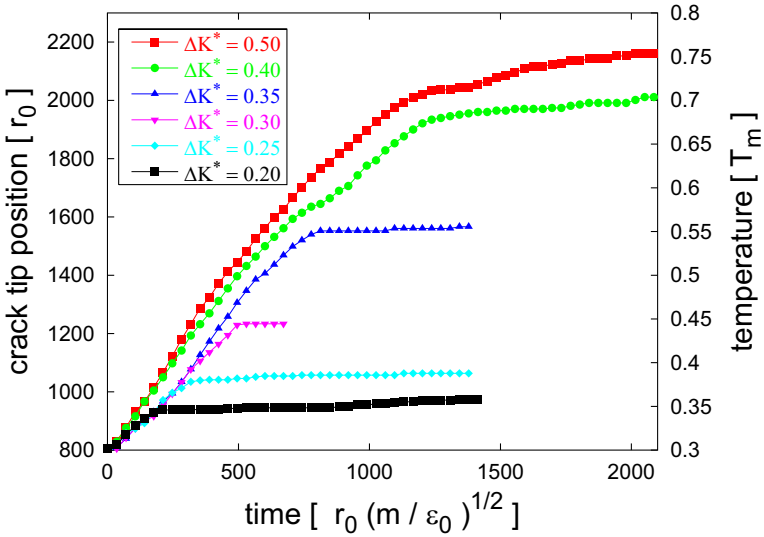

Figure 5.13: *Position of the crack tip over simulation time for simulations with temperature gradient.*

act as obstacles for moving dislocations. In contrast to the dislocation-emission-phason-wall mechanism in the low temperature regime, the blunting dislocation is able to shield the crack from the applied load and the crack does not follow the path of the dislocation. The crack tip requires sufficiently high opening stresses to follow the dislocation. In the case of the blunting dislocation the opening stress is apparently too small on the highly inclined glide plane.

For loads above $\Delta K^* = 0.40$ the blunting dislocation is no longer able to shield the crack. We still observe the nucleation of blunting dislocations but in contrast to the behavior for smaller overloads a new crack is formed from the dislocation core. As a result the crack is driven into the high temperature regime.

At temperatures above 70% of T_m the velocity of the crack drops considerably but the crack does not stop. This can be clearly seen in Fig. 5.13. The terminal velocity is about 10% of the velocity for brittle crack propagation. The decrease in velocity corresponds to a change in the mech-

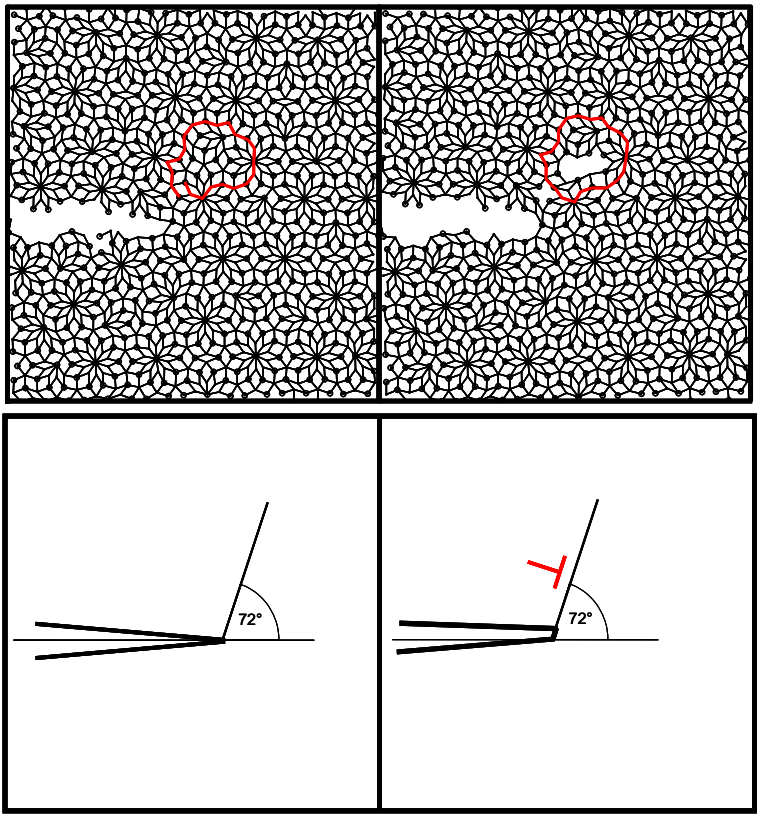

Figure 5.14: *Crack before (left) and after (right) blunting in the medium temperature regime at about 45 %T_m. The glide plane of the dislocation is inclined by 72° to the initial fracture plane. The Burgers vector of the blunting dislocation is visualized by the Burgers circuit.*

anism of crack propagation. Fig. 5.15 shows sections of configurations at three different times from a simulation at 75% of the melting temperature. The crack does no longer propagate with an atomically sharp crack tip but rather extends by nucleation, growth and coalescence of

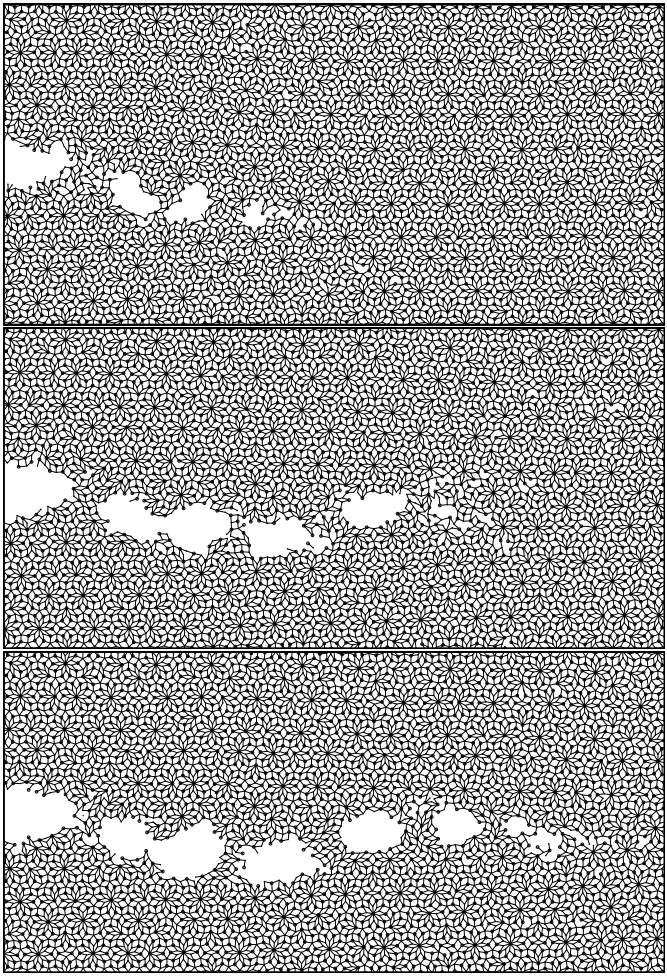

Figure 5.15: *Propagation mechanism in the high temperature regime at about 75% of T_m. The crack propagates by nucleation, growth and coalescence of microvoids in front of the crack tip.*

microvoids in front of the crack tip. Obviously the crack does not follow a favored fracture plane.

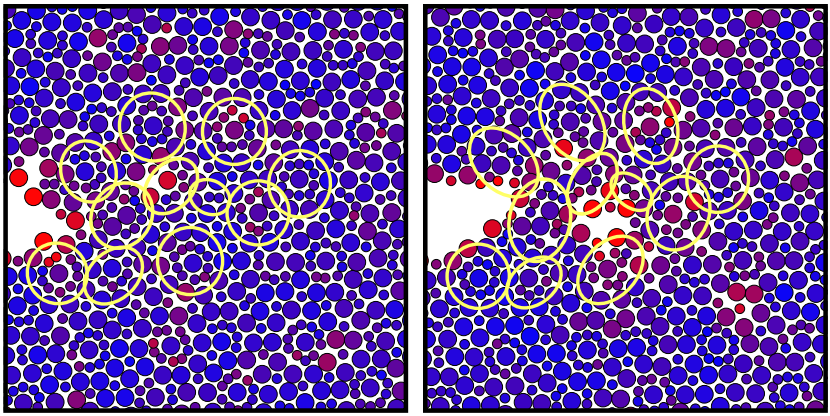

Figure 5.16: *Section from a simulation at 75% T_m before and after the nucleation of a void in front of the crack tip. The ovals indicate the direction of deformation of localized regions.*

The formation of voids in front of the crack tip has to be connected with plastic deformation in the vicinity of the crack tip. In the low temperature regime the crack tip plasticity is mediated by dislocations. Dislocations in our model quasicrystal travel on well defined crystallographic planes and are always followed by phason walls. The phason walls and the dislocations are clearly visible in the bond representation by the occurrence of forbidden local environments (see Fig. 5.11). In the high temperature regime we do not observe such distinct local atomic surroundings. Therefore we can exclude dislocation motion as the mode of plastic deformation. However, the number of breaking bonds in front of the crack is increased as can clearly be seen from figure Fig. 5.15.

Fig. 5.16 shows sections from a simulation at about 75% of the melting temperature in the atomic representation. The atoms are colored according to their order parameter. Due to the thermal vibrations of the atoms the order parameter shows large fluctuations even for regions far away from the crack. Thus the order parameter that was used successfully for low temperatures cannot be applied here to identify the regions of plastic deformation.

There exist various methods to detect microscopic deformation events in amorphous systems [105,106]. These methods do not require an ideal reference structure and should therefore be particularly suitable to detect defects that cannot be characterized as lattice defects. However, the techniques are based on the calcuation of atomic level stresses and local symmetry coefficients. Just like the order parameter, these values show large fluctuations at elevated temperatures. Therefore these methods cannot be applied to detect the microscopic deformations at elevated temperatures.

To nevertheless study the mechanisms that cause the change in the propagation mechanism and to identify particularly the structure elements that are responsible for the growth of the microvoids the atomic environments in front of the crack are inspected every 500 timesteps. Fig. 5.16 shows a section from a simulation at about 75% of the melting temperature before and after the nucleation of a void. It turns out, that the plasticity is mediated by localized atomic rearrangements. The rearrangements occur within very localized regions with a diameter of approximately $2r_0$. The ovals indicate the direction of the deformation in selected regions.

Similar rearrangements were observed in simulations of fracture and plastic deformation in amorphous model solids [107, 107]. Such rearrangements were proposed to mediate the plastic deformation in metallic glasses [108,109] and form the basis for models of viscoplastic deformation in amorphous solids [110].

The simulations in the high temperature regime imply that the change in the propagation mechanism is connected to the occurrence of the localized shear deformations. On the one hand, the shear transformations reduce the opening stress in front of the crack tip.

On the other hand, the absence of dislocations may also be attributed to these localized deformations. Simulations of dislocation motion in the same model system show clearly that dislocations at low temperatures travel on planes in between the clusters without intersecting these tightly bound structural units. However, in our simulations the shear transfomation zones occur even within the clusters.

The nucleation of a dislocation from the crack tip requires a sufficiently high shear stress on the glide plane. The local rearrangements in front of the crack may reduce the shear stress on the glide plane below the critical stress for dislocation nucleation. As a result the dislocation nucleation process is suppressed and the plastic deformation occurs by repeated local rearrangements in the shear transformation zones.

5.4 Discussion

The aim of the current work was to study the brittle-to-ductile transition in quasicrystals. On the macroscopic scale the brittle to ductile transition is a complicated phenomenon that depends not only on the material under consideration and the temperature but also on the loading rate and the microstructure of the solid. Obviously the large variety of phenomena where processes on many different length scales are envolved cannot be entirely understood by modelling the atomic scale. The studies were restricted to simple two-dimensional systems to elucidate the atomistic features that are important for the understanding of the brittle-to-ductile transition. Although our model system is very simple, there are some key features that do not depend on the distinct model system and should therefore be valid for a wide class of real quasicrystals.

By inspecting the stress distribution around the stable crack one finds that the crack field is confined to a circular region around the crack tip with a radius that is about the width of the sample. The surfaces at the pre-cracked side of the strip are fully relaxed. Far ahead of the crack tip the strip is homogeneously strained. Thus the geometry is suitable to study crack propagation under condition of a constant energy release rate. For our choice of the sample dimensions the crack advance can be followed for a length of about $300\, r_0$ before the crack "feels" the fixed boundary in front of the crack.

However, the limiting factor for the aspect ratio and consequently for the time the crack propagation can be observed without perturbations from the boundaries is given by the crack tip velocity. We observe crack tip velocities ranging from $10 - 60\%$ of the shear wave velocity.

Thus the crack can only be followed for a length of $40 - 80\,r_0$ before the first shock wave emanating from the crack tip is reflected from the fixed boundary and reaches the crack tip. Application of the stadium boundary conditions allows to enlarge this length to about $100\,r_0$ which is long enough to ensure that the crack can "scan" a sufficiently large number of different atomic surroundings. The characteristic features like the deviation of the crack are observed before the first wave that is reflected from the fixed boundaries reaches the crack tip. Thus an influence of the fixed boundary can be excluded as the origin for the deviation from the initial fracture plane.

5.4.1 Low Temperature Propagation

The major result from the simulations in the low temperature regime is that both model quasicrystals fail by brittle fracture. This is in good agreement with experimental studies which show that decagonal quasicrystals are brittle for low temperatures [9].

In the perfectly ordered quasicrystals, propagation is strongly influenced by the characteristic features of the model quasicrystals, namely the pronounced plane structure and the strongly bound decagonal clusters. The crack propagates on well-defined crystallographic planes and is strictly circumventing the tightly bound decagonal clusters. The resulting fracture surfaces show characteristic deviations of 36° to the initial fracture plane. The random tiling does not show a distinct plane structure. Here the resulting fracture surfaces show no distinct deviations from the initial fracture plane.

Simulations of crack propagation in periodic crystals show that the cracks possess a finite stability range. This is explained by the so-called lattice trapping effect. It causes the crack to be stable and not to advance until loads are applied that are somewhat larger than the Griffith value. The effect depends strongly on the structure and the interaction potential [30]. The trapping is expected to be small for closely packed structures and soft interaction forces but should be more pronounced for open structures and stiff potentials [30]. Quasicrystals are topologically densely packed structures. The Lennard-Jones potential used in

the current work is rather soft. Thus the lattice-trapping effect is expected to be less pronounced.

Indeed, we find that the stability range in our model quasicrystals is small. By increasing the load step-wise from the critical load we find that the crack can only be loaded to about $\Delta K^* = 0.01$ without propagation. However, for small overloads up to $\Delta K^* = 0.2$ the crack propagates only a few atomic distances r_0 and then stops. The cracks are stopped by obstacles like the incomplete cluster marked in Fig. 5.9 that are contained in both systems. Thus the stability range is rather determined by the inhomogenity of the structure and the distribution of local obstacles than by the influence of the lattice. From this it follows that the critical load is not unique but depends strongly on the position of the crack tip.

Another implication from the low temperature simulations is that the propagation is strongly influenced by the local atomic arrangement in front of the crack tip. This can be seen from the fact that the cracks in the perfecly ordered systems do not propagate along the initial fracture plane but deviates. The surface energy of the resulting fracture plane exceeds the one of a surface obtained by cutting the sample along a flat plane. Thus the fracture path in quasicrystals cannot be predicted by continuum considerations.

Although both models, the perfectly ordered and the random tiling quasicrystals, fail by brittle fracture in the low temperature regime, it turned out that the reason for the brittleness differs significantly for the two systems. The dislocation nucleation that was observed in the perfectly ordered systems does not increase the fracture toughness. The phason wall in the wake of the dislocation serves as a preferred path for the crack. In contrast to this in the random tiling system we do not observe the nucleation of dislocations from the crack tip. Here the brittleness is due to the loss of a plane structure that makes the dislocation nucleation impossible.

The simulations along the phason walls for different Burgers vectors show clearly that both the dynamics of the crack tip and the morphology of the resulting fracture surface are strongly influenced by the magnitude of the Burgers vector. For Burgers vectors with small components $b^{\parallel}$ in

physical space the phason wall serves as a prefered path for the moving crack and the crack follows the phason wall. For large components $b^{\parallel}$ the crack does not propagate on the phason wall, but deviates just like for the systems without phason wall. This suggests that phason walls that may be present in the structure due to frozen-in dislocations do not necessarily lower the fracture toughness. Again the propagation is strongly influenced by the occurence of obstacles like incomplete tenfold clusters in front of the crack tip. This can clearly be seen by comparing the simulations along phason walls with $b^{\parallel} = 1.8$ and $b^{\parallel} = 4.9$. For $b^{\parallel} = 1.8$ crack propagation is faster than for $b^{\parallel} = 4.9$. Moreover for $b^{\parallel} = 1.8$ the crack follows the phason wall whereas for $b^{\parallel} = 4.9$ it deviates just like for simulations without phason wall. However, the difference in surface energy for the two phason walls is less than 0.1%. Thus this change in mechanism cannot be explained by continuum considerations.

5.4.2 Medium and High Temperature Propagation

For temperatures about $30\%T_m$ crack propagation was studied using the strip geometry with temperature gradient. Although this method was applied exclusively for two-dimensional models an extension to three-dimensional systems is straightforward. However, the number of atoms needed to establish the temperature gradient and particularly to simulate a wide range of temperatures is rather high.

Although we have scaled the system according to the thermal expansion of the sample the change in the elastic constants was not taken into account. The elastic constants and consequently the load level changes with temperature. Thus the load level is not constant over the sample. However, it turned out that the method is suitable to investigate the transitions with temperature qualitatively.

In the medium temperature regime we observe a spontaneous blunting of the crack tip by nucleation of dislocations on planes that are inclined by 72° to the initial fracture plane. For the highly inclined blunting dislocation the crack does not follow the dislocation.

The stress field of the blunting dislocation shields the forces acting on the crack tip. The magnitude of the shielding is a strictly monotonic

function of the distance between the crack tip and the core of the dislocation. We observe that the dislocation does not get farther away from the crack tip than about $5r_0$ where it is blocked by an obstacle. Thus the shielding is particularly high and the crack is arrested by the blunting dislocation. Although the spontaneous blunting yields to a crack arrest for small overloads, for large overloads the blunting dislocation is not able to shield the crack.

Whether a crystalline material is brittle or ductile depends not only on the ability to emit dislocations but also on their mobility. When a dislocation nucleates it is driven away from the crack tip by the stress field of the crack tip. The blunting dislocation produces a back stress that prevents the crack tip from further dislocation emission. The strength of this back stress depends on the distance of the dislocation from the crack tip. For further nucleation the leading dislocation has to move sufficiently far away from the crack tip to reduce the back stress until stresses at the crack tip are sufficiently high for nucleation of the next dislocation.

In our simulations the blunting dislocation blocks the crack tip from further dislocation emission. Thus for larger overloads the stress cannot be reduced efficiently to arrest the crack by repeated emission of blunting dislocations. As a result the crack is driven into the high temperature regime.

Studies of the brittle to ductile transition in periodic crystals show clearly that sources near the crack tip may play an important role for the development of a plastic zone around the crack tip. In our simulations the only source for dislocation nucleation is given by the crack tip. However, the immobility of the dislocations due to structure intrinsic obstacles should limit the development of the plastic zone independently from the mechanism of the dislocation generation. This is another indication that limited dislocation mobility due to the structure intrinsic obstacles is responsible for the pronounced brittleness at low temperatures and the high brittle to ductile transition temperatures.

For high temperatures above $70\%T_m$ we observe that the crack tip velocity drops considerably. The drastic decrease in the propagation velocity is connected to a change in propagation mechanism. The simulations

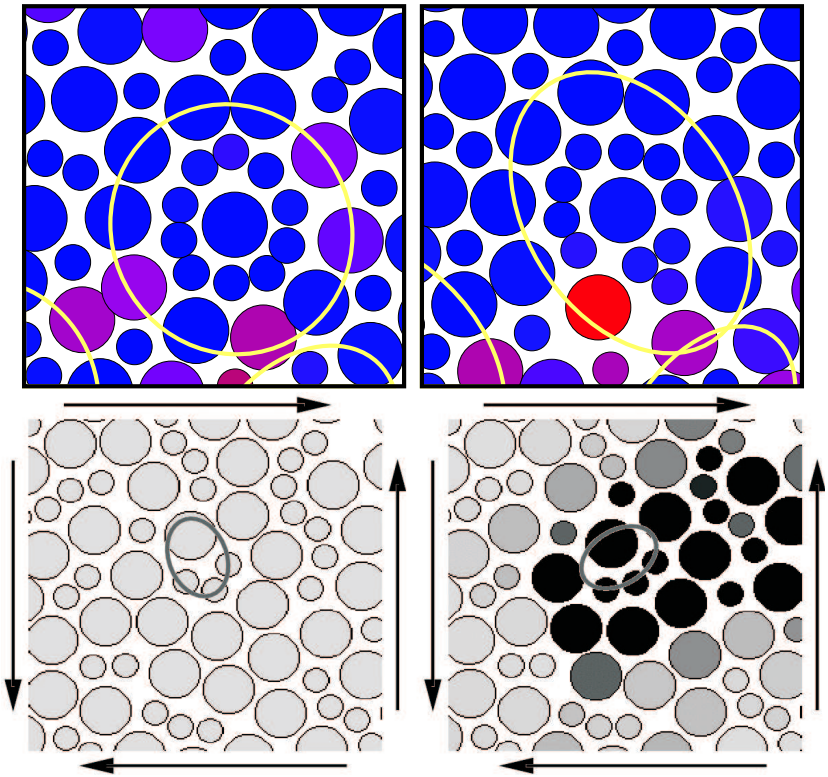

Figure 5.17: *Close up from a shear transformation zone form the simulation in decagonal model quasicrystal (top) and a simulation of deformation in a model amorphous solid [56] (bottom).*

show clearly that the change in mechanism is not connected to an increase of plastic deformation by an increase of the dislocation activity in front of the crack tip as one would expect for periodic systems. Thus the change in the propagation mechanism should not be confused with a brittle to ductile transition as it is observed in periodic crystals.

The fracture modes are very similar to those observed in model non-crystalline solids [56, 110]. In these simulations the cracks do not prop-

agate by brittle fracture but rather by nucleation, growth and coalescence of microvoids. The plastic deformation in the amorphous systems is mediated by localized atomic rearrangements, so-called shear transformation zones. These zones are very similar to those observed in the high temperature simulations in the model quasicrystals. Thus the simulations suggest that the influence of the plane structure is suppressed for high temperatures.

In conclusion at low temperatures the crack propagates along crystallographic planes just like in periodic crystals, whereas a glass-like behaviour is dominant at high temperatures.

5.5 Summary I (Decagonal Quasicrytals)

Crack propagation of two-dimensional model quasicrystals was studied over a wide range of temperatures by means of molecular dynamics simulations. For this purpose a new simulation geometry was applied that allows to study the changes in mechanisms of dynamic crack propagation with temperature. The simulations reveal that the understanding of the complex phenomena that occur in dynamic fracture of quasicrystals demands studying crack propagation on the atomic scale.

The most important results are:

- The propagation for low temperatures is strongly influenced by the local atomic arrangements in front of the crack tip. Obstacles like complete or incomplete clusters impede the motion of the crack.
- Dislocation emission does not increase the fracture toughness because of the phason wall in the wake of the dislocation.
- The propagation along phason walls depends strongly on the arrangements of defects on the phason wall and thus on the associated Burgers vector. As a result, frozen dislocations do not necessarily lower the fracture toughness.
- For medium temperatures we observe spontaneous blunting of the crack tip by dislocation emission. The blunting dislocations are blocked by structure intrinsic obstacles. Although this results in an

increase of fracture toughness the dislocation blocks the crack tip from repeated dislocation nucleation.

- At elevated temperatures a glass-like ductile growth mode is dominant where the crack propagates by nucleation, growth and coalescence of microvoids in front of the crack.

The most obvious perspective for future studies of crack propagation in decagonal systems is to extend the simulations to three-dimensional models. Particularly the influence of the dislocations is expected to be different in a three-dimensional system. In the two-dimensional model, dislocations can only be nucleated and propagate as perfectly straight edge dislocations, whereas in three-dimensional systems nucleation of dislocation loops with a mixed edge-screw character is possible. Although the nucleation process may differ for three dimensional systems, such dislocations are also followed by phason walls similar to those observed in our models. The clusters are expected to act as obstacles for the dislocations just like in the two-dimensional systems. Thus, even if dislocation emission is possible for three-dimensional systems, the shielding of the crack tip should also be reduced due to the influence of the phason wall.

Although there are some realistic structure models for decagonal quasicrystals it is not feasable to study crack propagation in these systems by means of molecular dynamics. The major difficulty is the need for an appropriate interaction model. Even though there exist some semi-empirical potentials for decagonal quasicrystals, these are pure bulk potentials which are inadequate for simulations of crack propagation. The requirements for potentials to study crack propagation are rather high. Potentials are needed which reproduce not only the bulk properties of the system, but also allow to model free surfaces. Moreover, it should be valid for the large strains at the crack tip. There are some attempts to develop such potentials, however, at the moment such potentials that fulfill all these requirements are not available.

Chapter 6

Crack Propagation in Icosahedral (3D) Quasicrystals

In this chapter the results of a series of simulations in icosahedral model quasicrystals is presented. The simulations have been performed in collaboration with Frohmut Rösch who did his diploma thesis on crack propagation in icosahedral quasicrysals [111]. This chapter focuses on the most important results of these simulations and on the influence of the clusters on the morphology of the fracture surfaces in particular.

6.1 Icosahedral Model Quasicrystals

As mentioned before icosahedral quasicrystals show quasiperiodic order in three dimensions, which cannot be reduced to simple two-dimensional model systems. The simulations are carried out for a three-dimensional binary model quasicrystal introduced in section 2.5.2. The atomic interactions are modeled by Lennard-Jones potentials. As for the two-dimensional structures the depths of the LJ potentials are ϵ_0 and $2\epsilon_0$ for atoms of the same and different types, respectively. As unit of length we use the nearest neighbor distance r_0 of two small atoms in the structure. This is a very simplistic model quasicrystal, but it nevertheless should produce the correct qualitative behavior of crack propagation in close-packed quasicrystals like icosahedral $(Al,Zn)_{63}Mg_{37}$. The same model system was used for molecular dynamics simulations of shock waves [112, 113] and dislocation motion [114, 80].

The model system is elastically isotropic. The elastic constants were calculated by deformation of an approximant containing about 40,000 atoms. The shear modulus was calculated to $\mu = 41.1\epsilon_0/\sigma^3$ from the slope of a stress-strain curve in a simple shear deformation. The bulk modulus was calculated to K=$94.9\epsilon_0/\sigma^3$.

As the decagonal model quasicrystals, the icosahedral model quasicrystals show two characteristic features of real quasicrystals, namely a pronounced plane structure and clusters. The clusters are given by a small center atom surrounded by two shells. The first one contains 12

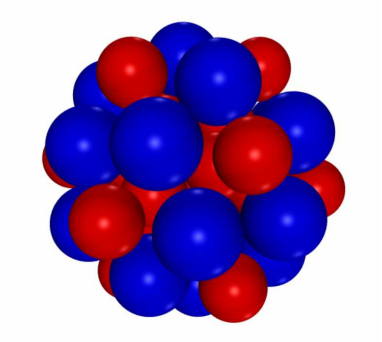

Figure 6.1: *Bergman Cluster contained in the IBT.*

small atoms that are arranged on the corners of an icosahedron. The outer shell is formed by 20 large and 12 small atoms that are placed on the corners of a pentagonal dodecahedron and an icosahedron, respectively. This arrangement of 55 atoms is the so-called Bergman cluster. Bergman clusters are the basic structure element of a closely related crystalline (Al,Zn)Mg structure where they form a body-centered-cubic packing [115].

As for the two-dimensional systems we start by analyzing the surface energy of the systems for different crystallographic orientations. We relax a specimen and split it into two regions. Subsequently, the two parts are shifted rigidly by a distance of $10r_0$ perpendicular to the cutting plane. The surface energy is then calculated from the difference of the artificially cleaved and the undisturbed specimen.

Fig. 6.2 shows the surface energy for three different orientations as a function of the position of the cutting plane. We find a pronounced plane structure of low and high surface energies along twofold directions. The planes of lowest surface energy occur with two separations, forming a Fibonacci chain. Along the fivefold direction the plane structure is less pronounced, but we still find planes of low surface energy, whereas for the threefold direction there is no such distinct plane structure. For our simulations we select as initial fracture planes surfaces of lowest energy for the respective orientation. In this thesis we restrict ourselves to

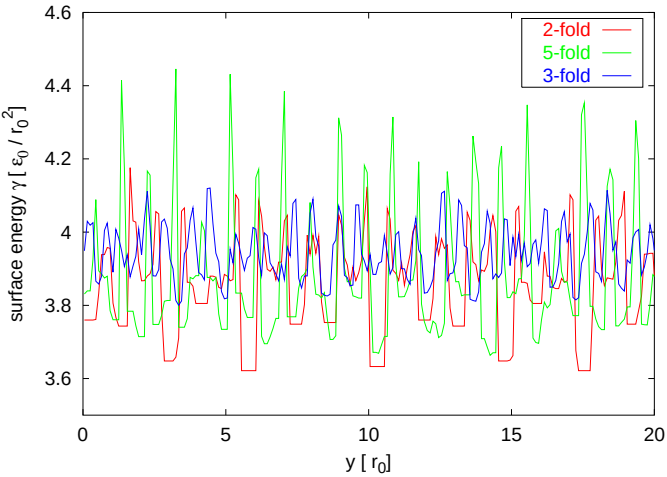

Figure 6.2: *Surface energy in dependence on the cutting plane perpendicular to two-, three- and fivefold directions.*

fracture planes perpendicular to two- and fivefold directions. For results of simulations along other directions we refer to [111].

6.2 Visualization

There are two essentially different types of data that can be used for the visualization of a molecular dynamics simulation. The first possibility is to compute the distribution of certain scalar quantities like the kinetic energy density, which is evaluated on a regular grid and then displayed with a volume renderer. Fig. 6.3 shows such a volume data set of the kinetic energy. Regions of low intensity are rendered with high transparency. Sound waves emitted by the propagating crack are clearly visible. In most cases, however, volume data are often too homogenous and show little contrast, so that not much can be seen.

Volume data sets represent, by their very nature, a continuous distribution of some locally averaged quantity. For this reason, they are not suited for the elucidation of microscopic processes. To study crack propagation on an atomistic level, it is necessary to render selected atoms

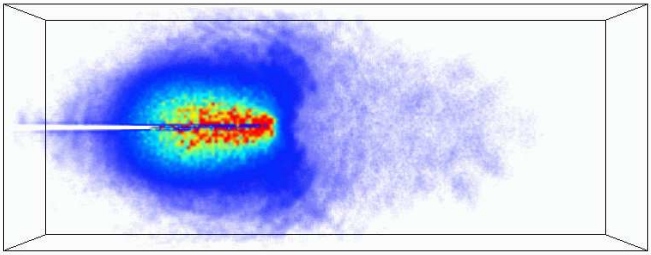

Figure 6.3: *Volume visualization from a simulation in the IBT.*

only. Just like in the two-dimensional case, in icosahedral quasicrystals the atoms have largely varying local environments. Their potential energy thus varies significantly from atom to atom, even for atoms of the same type in a defect-free sample. Defects can therefore not be visualized by applying a simple energy cut-off as in periodic systems.

The method that was applied here uses the coordination number for the data selection. The coordination number is evaluated by counting the number of atoms within a certain distance. This cut-off distance is configurable and may depend on the type of the atoms involved. Like the potential energy, the coordination number varies from atom to atom, but to a much smaller degree. In a perfect sample, it is 12 or 13 for the small atoms, and ranges from 14 to 16 for the large atoms. Atoms near a defect have a significantly lower or higher coordination number, so that it is possible to visualize fracture surfaces and dislocation cores by displaying only atoms outside an suitable interval of coordination numbers. Fig. 6.4 shows a snapshot of a simulation with 4 million atoms, where atoms are displayed if their coordination number is less than 12 for small atoms, and less than 14 for large atoms. With this method, the number of atoms to write to the output files could be reduced by three orders of magnitude, which allows to take more frequent snapshots instead. Although this method is particularly suitable to detect fracture surfaces it is by no means restricted to the detection of free surfaces but applies also for dislocations and phason walls.

Detailed analysis of the coordination number shows that about 85% of the small atoms have 12 nearest neighbors. The distribution of the

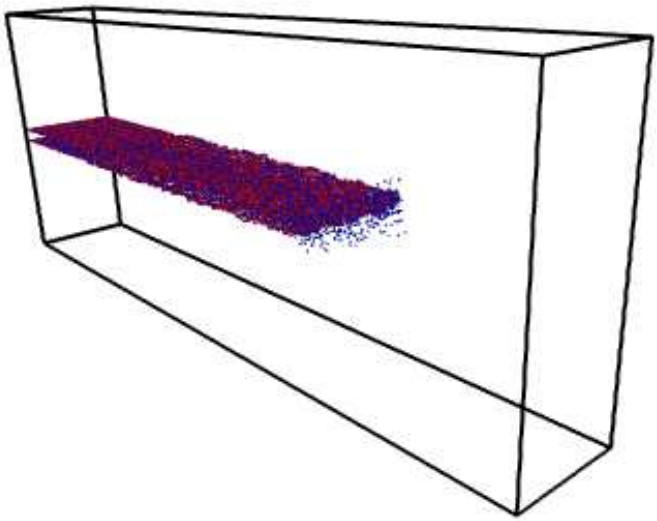

Figure 6.4: *Crack in the IBT in atomic resolution.*

nearest neighbor configurations for the small atoms is shown in Fig. 6.5, where n_L and n_S denotes the number of small and large nearest neighbours respectively.

6.3 Simulation Geometry

Since we are interested in the morphology of fracture surfaces we use a geometry that allows us to follow the dynamics of the running crack for a long time. For this purpose, we use a strip geometry which is the straightforward extension of the geometry used for the two-dimensional simulations. The samples consist of about 4 million atoms, with dimensions of approximately $450r_0 \times 150r_0 \times 60r_0$. Periodic boundary conditions are applied in the direction parallel to the crack front. For the remaining directions, all atoms in the outermost boundary layer of width $2.5r_0$ remain fixed during the simulation. Just like in the two-dimensional models, the system is initially strained to the Griffith load where the energy release rate G is equal to the surface energy of the

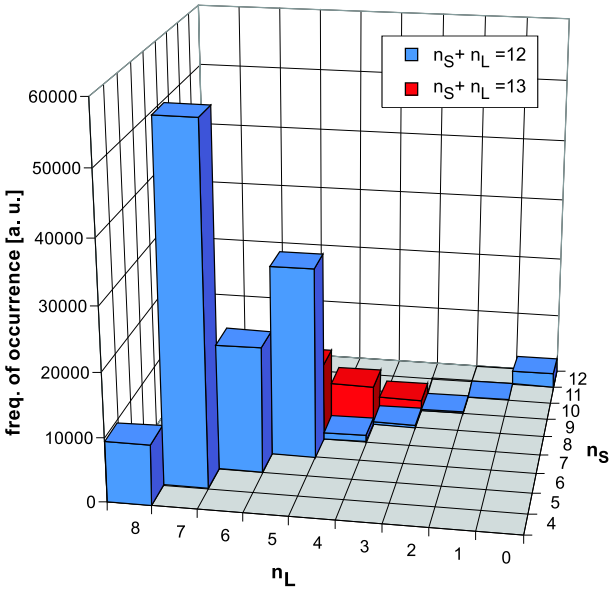

Figure 6.5: *Distribution of the nearest neighbor configurations for the small atoms in the model quasicrystal.*

two crack surfaces, 2γ. Subsequently the sample is relaxed and loaded according to the procedure described in Section 4.3.

In this work, we concentrate on exploring crack propagation without thermal fluctuations. Thus we set the initial temperature to 10^{-4} of the melting temperature T_m, which is close to zero temperature. Afterwards the crack is loaded by adding a fraction of the displacement field to the stable crack. The answer of the system is followed by molecular dynamics simulations. The overloads are given by ΔK^* in the following, which is the relative fraction of the stress intensity factor due to the displacement field that is added to the stable crack.

In contrast to the two-dimensional case the ability of a crack to emit a dislocation in a three-dimensional system depends not only on the orientation of the cleavage plane with respect to the glide plane but also on the boundary conditions along the crack line. By applying periodic

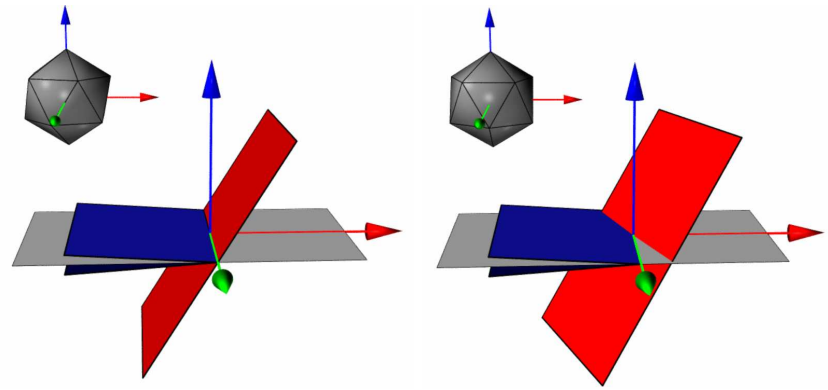

Figure 6.6: *Orientations of the potential glide planes with respect to the cleavage plane for propagation parallel (right) and perpendicular (left) to a twofold direction on a cleavage plane perpendicular to a fivefold direction.*

boundary conditions along the crack front the maximum shear stress occurs in a plane that contains the crack front and is inclined to the cleavage plane. Simulations of dislocation motion [114, 80] in the same model system show that the primary slip systems are given by glide planes perpendicular to twofold axis with Burgers vectors in twofold directions. Fig. 6.6 shows a schematic of the simulation geometry for propagation on a cleavage plane perpendicular to a fivefold axis. The icosahedron indicates the orientation of the symmetry directions with respect to the simulation geometry.

For propagation direction perpendicular to an axis with twofold symmetry (Fig. 6.6 left) the glide plane with the largest resolved shear stress contains the crack front and is inclined to the cleavage plane. For propagation along a twofold direction the potential glide plane is intersecting the crack front and is oriented oblique with respect to the cleavage plane.

The modes of dislocation nucleation from a crack tip is expected to depend on the orientation of the crack front with respect to the glide plane. To study the influence of the glide plane orientation and particularly whether dislocation emission is possible in the icosahedral model

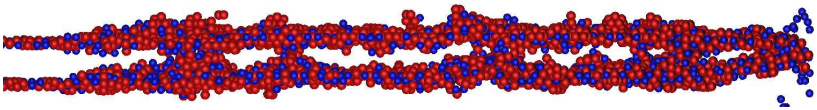

Figure 6.7: *Snapshot of a crack in atomic resolution.*

system, we have simulated propagation in different directions on essentially the same cleavage plane.

6.4 Results

6.4.1 Crack Tip Velocity

The major result of the simulations is that the icosahedral model quasicrystal fails by brittle fracture without any crack tip plasticity for all orientations of the cleavage plane. In contrast to the simulations in the two-dimensional model systems we do not observe the nucleation of dislocations from the crack tip.

For small overloads up to $\Delta K^* = 0.20$ we observe that the cracks propagate only a few atomic distances and stops, just like in the two-dimensional systems. The minimal velocity for brittle crack propagation is about 10% of the shear wave velocity v_s. For loads $\Delta K^* > 0.2$ the velocity increases monotonically with the applied load. The crack velocities are in a range of 10-45% of v_s.

6.4.2 Fracture Surface Analysis

Fig.6.7 shows a snapshot from a simulation of propagation on a twofold cleavage plane. The atoms at the fracture surface were selected according to their coordination number as described above. The blue and red atoms correspond to the large and small atoms respectively. Obviously the fracture surface is not flat but shows a pronounced roughness on the atomic scale. To analyze the morphology of the fracture planes, the height profiles of the fracture surfaces were calculated by simulating an idealized scanning microscope.

In a first step the two fracture surfaces are separated. Due to the roughness of the crack it is not possible to separate the surfaces by cutting the sample along a flat plane parallel to the cleavage plane as can clearly be seen from Fig. 6.7. However, a simple way to separate the two fracture surfaces can be found by inspecting the atomic displacements of the fractured sample with respect to an undisturbed configuration. Due to the mode I loading atoms in the upper and lower part of the sample carry positive and negative vertical components of displacements perpendicular to the cleavage plane, respectively. For the surface analysis the lower part of the sample was selected by removing all atoms that carry a positive vertical component.

Subsequently the height $h(\mathbf{r})$ is calculated as a function of the two lateral coordinates $\mathbf{r} = (x, y)$. For this purpose we scan the fracture surface with the tip of a virtual scanning probe microscope. The shape of the tip is assumed to be spherical with radius R. For simplicity, both, the tip and the atoms of the surface are approximated by hard spheres. The radii were chosen to be $0.52r_0$ for small atoms and $0.61r_0$ for the large ones.

For a given point $\mathbf{r} = (x, y)$ we calculate the boundary point of the tip and the surface atoms considering the different radii of the atoms and the spherical tip. The height is given by the center of the sphere that mimics the scanning tip. The fracture surface was scanned with a spatial resolution of $0.5r_0$ in both lateral coordinates and the radius of the tip was chosen to be $R = 2r_0$. Although this scanning method is oversimplified, the resulting height profile should be comparable to the one that would be measured by an atomic force microscope in atomic resolution.

6.4.2.1 Propagation along Twofold Planes

Fig. 6.8 shows the height profile of a simulation on a cleavage plane perpendicular to a twofold axis. The crack propagation direction is from the left to the right. The initial fracture surface is flat, as can be seen from the homogeneous regions on the left. The surfaces resulting from the propagation of the crack, however, show a pronounced pattern

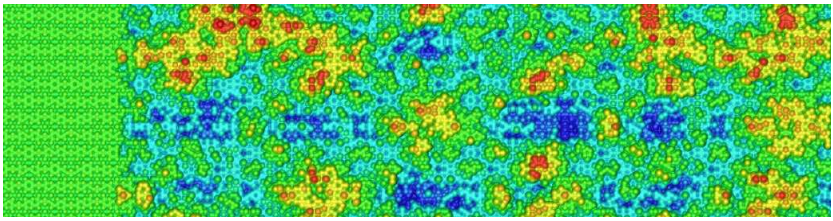

Figure 6.8: *Fracture surfaces from simulations perpendicular to a twofold axis.*

of regions with different heights with an average vertical roughness of about $4r_0$ which corresponds to the diameter of the icosahedral clusters.

To study the influence of the propagation direction we have selected two different directions of propagation along a five- and twofold symmetry axis, respectively. For both directions we find almost identical roughnesses of the fracture surface and the cracks do not deviate from the initial fracture plane.

6.4.2.2 Propagation along Fivefold Planes

For simulations on fivefold cleavage planes we have selected a plane of lowest surface energy perpendicular to a fivefold direction. The influence of the propagation direction was studied by choosing two different propagation directions perpendicular and parallel to a twofold direction. Fig. 6.9 shows the height profiles for the two directions at a load of $\Delta K^* = 0.3$. In contrast to the simulations on the twofold cleavage plane the crack does not propagate on the initial cleavage plane but deviates from it for both propagation directions as can clearly be seen from Fig. 6.9. Moreover, the morphology of the resulting fracture surfaces differ significantly in dependence on the propagation direction. For propagation parallel to a twofold direction the roughness of the fracture surface is even less pronounced than for propagation on a twofold cleavage plane. Propagation perpendicular to a twofold direction, however, results in a fracture surface that again shows regions of different heights. In contrast to the twofold cleavage plane we observe the formation of

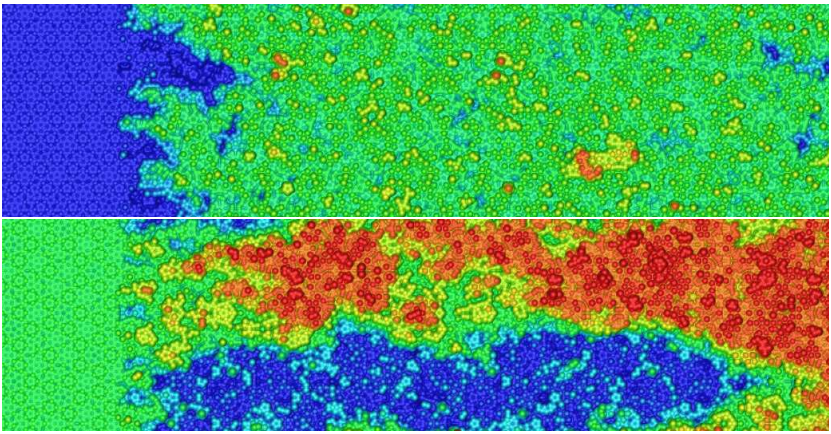

Figure 6.9: *Fracture surfaces from simulations on a fivefold cleavage plane for propagation direction parallel (top) and perpendicular (bottom) to a twofold axis.*

ledges. The height of the ledges is approximately $2r_0$ which corresponds to the diameter of the Bergman cluster.

6.5 Discussion

The major result from our simulation in icosahedral quasicrystals is that the system fails by brittle fracture. In contrast to the decagonal models we do not observe the nucleation of dislocations from the crack tip, irrespective from the orientation of the cleavage plane and the propagation direction. It should be noted here that the various orientations of the cleavage plane studied in the current work, should in principle allow for nucleation of dislocations on both, planes that are inclined and oblique to the initial cleavage plane. However, we do not observe any dislocation activity irrespective of the crystallographic orientation of the potential glide plane. Thus we conclude that the model quasicrystal appears to be an intrinsically brittle material. This is in good agreement with simulations of dislocation motion in the same model system which show clearly that the plasticity is limited particularly for low temperatures [79, 80].

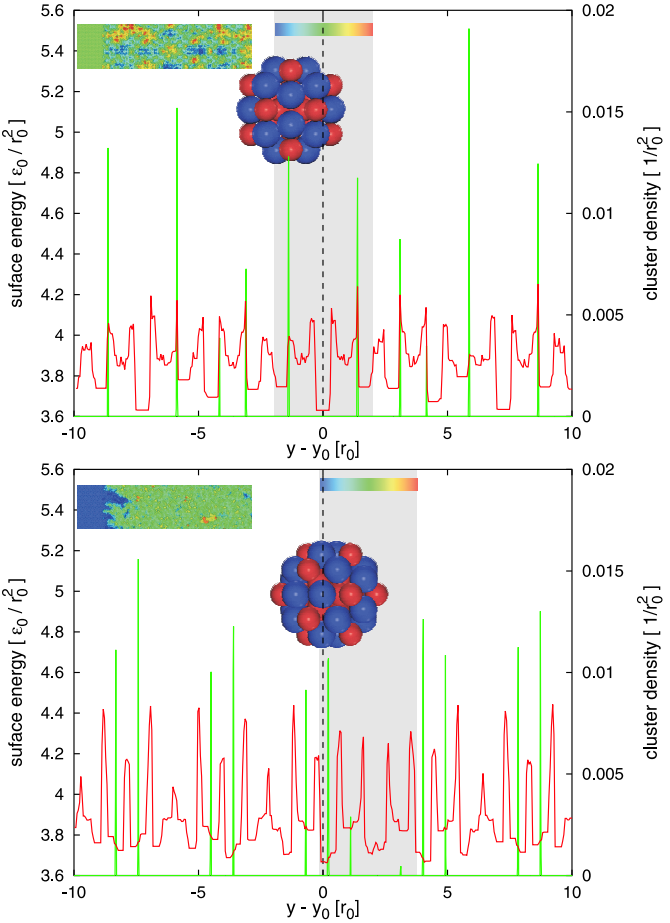

Figure 6.10: *Density of the clusters along a direction perpendicular to the cleavage plane. The initial fracture plane is indicated as a dashed line.*

The absence of dislocations in the icosahedral system seems also be reasonable compared to compression experiments in AlPdMn that clearly

show that icosahedral quasicrystals fail by brittle fracture up to temperatures of about 70% of the melting temperature.

Moreover, we find rough fracture surfaces comparable to those obtained experimentally by cleavage of AlPdMn icosahedral quasicrystals by Ebert *et al.* [4]. The roughness of the surfaces measured as the maximal difference in height from the surface profiles is about $4r_0$, which corresponds to the largest atomic separation of two small atoms within a Bergman cluster. The surface energies of the rough fracture surfaces created during the fracture process are about $10\% - 15\%$ higher compared to the corresponding surface energies of the atomically sharp surfaces of the flat seed cracks. This suggests that the morphology of the fracture surface is strongly influenced by the bond breaking process and consequently by the detailed arrangement of the bonds in front of the crack tip. From this it follows that the crack path and thus the morphology of the fracture surfaces cannot be explained by the Griffith criterion that is based on continuum considerations.

The experimentally observed roughness of the fracture in icosahedral AlPdMn is assigned to the so-called pseudo Mackay cluster of 51 atoms which forms the basis structure element in the structure model for icosahedral AlPdMn according to Boudard *et al.* [116]. The model quasicrystals used in the current work contain so-called Bergman clusters. We study the influence of these structure elements on the morphology of the fracture surface. For this purpose we identify those clusters that are intersected by the advancing crack. Unfortunately this information cannot be obtained by merely considering the fractured sample. When a cluster has been intersected, its atoms are distributed on the two fragments of the sample. After the crack has traveled through the sample it is impossible to decide which atoms where located within a cluster. In molecular dynamics simulations, however, we can follow the trajectory of each individual atom for the whole simulation. The basic idea is to use this property to reconstruct the path of the crack which is subsequently translated back into a reference sample without a crack. In this undisturbed sample the clusters can be easily detected geometrically by inspecting the number of nearest neighbors of different types. This makes it possible to analyze in detail, whether the clusters are intersected or circumvented by the moving crack. Moreover, the procedure

allows to determine in which way the clusters are intersected and which shell of the cluster is affected.

The cluster analysis was performed for the fracture surfaces perpendicular to five- and twofold directions. It turns out that the clusters are not strictly avoided, but to some extent intersected by the dynamic crack. Both, the frequency of the intersected clusters and the way the clusters are separated depends on the crystallographic orientation of the crack. However, the clusters are cut less frequently compared to the flat seed cracks for all orientations. This suggests that the the morphology of the fracture surface is indeed influenced by the clusters.

The Bergman clusters are located on families of parallel planes. Both the mean distances of adjacent planes and their occupation density vary for different crystallographic orientations. Thus the influence of the clusters is expected to vary also for different orientations of the cleavage plane. Fig. 6.10 shows the density of the cluster centers and the surface energy for planes parallel to two- and fivefold cleavage planes as a function of the coordinate perpendicular to the cleavage plane. The cluster density shows pronounced peaks of different heights, corresponding to planes of low and high cluster density. The dashed lines indicate the position of the initial fracture plane.

For propagation along twofold cleavage planes the initial fracture plane is located in-between two peaks of high cluster density which are separated by a distance of about $2.7r_0$. Since this distance is smaller than the diameter of the Bergman cluster the initial flat seed crack intersects the clusters above and below the initial fracture plane between the first and second shell of the cluster, separating two small and two large atoms, respectively (see Fig. 6.10 top).

Detailed analysis of the cluster intersections show clearly that clusters are cut less frequently by the dynamic crack compared to the atomically sharp surface of the flat seed crack. Thus the pronounced roughness of the fracture surfaces on twofold cleavage planes can be assigned to the clusters. For both propagation directions, the average height of the resulting fracture surface coincides with the initial fracture plane indicating that the crack propagates mainly on a plane in-between the planes of high cluster density.

Cracks on fivefold cleavage planes show a different behavior. For simulations where the propagation direction is chosen parallel to a twofold direction the crack deviates from the initial fracture plane as can clearly be seen from Fig. 6.9 (bottom). By comparing the average height of the flat seed crack on the left with the average height of the surface that results from the fracture process it turns out that the crack deviates from the initial fracture plane. The deviation may be explained by the distribution of the clusters within the structure. In contrast to the twofold direction, here the initial fracture plane is located very close to a plane of high cluster density. As a result the flat seed crack intersects a large number of clusters within the first shell (see Fig. 6.10 bottom). By deviating from the initial cleavage plane the crack reduces the number of intersected cluster drastically. Moreover the roughness of the resulting fracture surface is less pronounced, compared to the propagation on the twofold cleavage plane. This again suggests that the primary cleavage planes in icosahedral quasicrystals cannot be identified by merely considering the surface energy. Instead of this the distribution of the clusters has also to be taken into account.

6.5.1 Comparison with Experiments

Experiments on crack propagation in quasicrystals are scarce. Most of the experiments were performed in icosahedral AlPdMn where single quasicrystals of centimeter-size are available. However, to study crack propagation under well defined loading conditions large single crystals are needed which are still rather delicate to produce even for AlPdMn. The model used in the current work is a structure model for . Thus the results are not directly comparable to the experiments performed in AlPdMn. Nevertheless, our model shows some properties, like the occurrence of clusters and a pronounced plane structure, which are common to all icosahedral quasicrystals. Particularly the distribution of the clusters in AlPdMn [117] appears to be similar to that in our model system. Thus the results should be at least in a qualitative way comparable to the experiments in AlPdMn.

Most of the experiments are indentation tests in icosahedral AlPdMn. The extreme brittleness of icosahedral quasicrystals at low temperatures

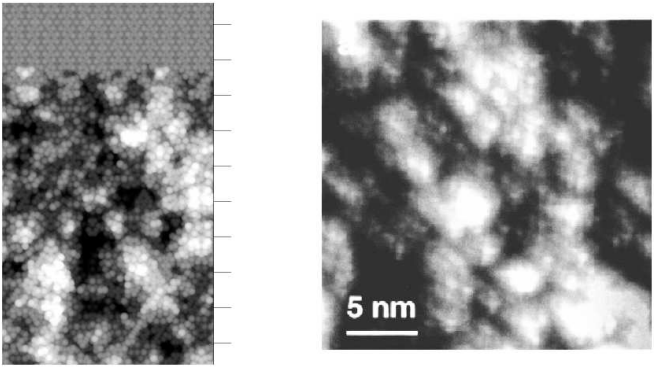

Figure 6.11: *Comparison of the fracture surface on twofold cleavage planes. Both, experimentally observed (left) [4] and the surface from simulation of dynamic crack propagation show a pronounced roughness on the atomic scale.*

manifests itself in the occurrence of microcracks emitted from the indenter corners [28, 118, 119, 120]. This is in agreement with our simulations which show that our model system appears to be intrinsically brittle at low temperatures.

The morphology of fracture surfaces in polycrystalline AlPdMn at room temperature [118] suggests that the fracture mode is not given by intergranular fracture. The observed surface steps form angles of 108° suggesting that the samples fractured by cleavage on fivefold planes. Fivefold cleavage planes with crystal-like planar fracture surfaces were also observed in samples of icosahedral AlPdMn quasicrystals crushed for neutron and x-ray studies [116]. Besides the fivefold cleavage planes, fracture surfaces oriented normal to twofold axis have also been observed [119, 116]. The occurence of five- and twofold planes as primary cleavage planes is in accordance with our simulations.

The surfaces of AlPdMn single crystals obtained by cleavage fracture in ultrahigh vacuum were studied by Ebert *et al.* [4] by means of scanning tunneling microscopy. The authors observed macroscopically flat and smooth surfaces with rough structure on the nanometer scale. Fig.6.11 shows the fracture surfaces on twofold cleavage planes. Both, the ex-

perimentally observed (Fig.6.11 right) and the surface obtained from simulation of dynamic crack propagation show a very similar roughness. Although the experimentally observed contrast is not directly transformable into a hight contrast, the accordance between the simulated and the experimentally observed surfaces suggests that at least the lateral featurs are reproduced by our simulations. A similar agreement is found for the fivefold surfaces. However, in our simulations the roughness of the fivefold surfaces is less pronounced which is not observed experimentally.

6.6 Summary II (Icosahedral Quasicrystals)

Propagation of mode I cracks have been studied by means of molecular dynamics simulations. For this purpose samples of about 4 million atoms were endowed with atomically sharp seed cracks on two- and fivefold cleavage planes. Subsequently the system was loaded by linear scaling of the displacement field and the response of the system was monitored by molecular dynamics simulations.

The most important results are:

- We observe brittle fracture without any crack tip plasticity irrespective of the orientation of the cleavage plane and the propagation direction.
- The fracture surfaces are not flat but show a pronounced roughness on the atomic scale, comparable to that observed experimentally. The magnitude of the roughness depends on both the cleavage plane and the propagation direction.
- The clusters inherent in the structure are not strictly circumvented but are cut to some extend by the moving crack. However, for all cleavage planes the clusters are cut less frequently compared to the flat seed cracks irrespective of the propagation direction. Thus the roughness of the fracture planes can be assigned to the occurrence of the clusters.

6.7 Outlook

Our simulations of crack propagation in a three-dimensional system show clearly that the fracture process in icosahedral quasicrystals is influenced by obstacles like the icosahedral clusters. The strength of these structure intrinsical obstacles is expected to depend strongly on the interaction potential. In the two-dimensional systems the parameters for the LJ potentials were chosen in such a way that the highly coordinated decagonal clusters are the tightest bound structural units. In the three-dimensional case it is far from obvious which choice of the potential favors the Bergman clusters as tightly bound structural units of the quasicrystal. Thus one route to be followed in future simulations may be to study whether the strength of the structure intrinsical obstacles can be tailored by varying the parameters of the LJ potentials.

In the current work the simulations were performed by using simple model systems with generic pair interactions. Thus another direction for further investigations is to model crack propagation with more realistic atomic interactions. However, although there exist a large variety of semiempirical potentials for metals and semiconductors, material-specific interactions are currently not available for quasicrystals. There are attempts to compute semi-empirical potentials by using ab-initio calculations. Such potentials may be useful for a deeper understanding of the fracture process in quasicrystals.

List of Figures

Bibliography

[1] D. Shechtman, I. Blech, D. Gratias, and J. W. Cahn, Metallic Phase with Long-Range Orientional Order and No Translational Symmetry, *Phys. Rev. Lett.* **53** (1984) 1951–1953.

[2] Ch. Rudhart, P. Gumbsch, and H.-R. Trebin, Crack propagation in perfectly ordered and random tiling quasicrystals, *J. Non-Cryst. Solids* **334 & 335** (2004) 453–456.

[3] R. Mikulla, J. Stadler, F. Krul, H.-R. Trebin, and P. Gumbsch, Crack Propagation in Quasicrystals, *Phys. Rev. Lett.* **81** (1998) 3163–3166.

[4] P. Ebert, M. Feuerbacher, N. Tamura, M. Wollgarten, and K. Urban, Evidence for a Cluster-Based Structure of AlPdMn Single Quasicrystals, *Phys. Rev. Lett.* **77** (1996) 3827–3830.

[5] R. Mikulla, J. Stadler, P. Gumbsch, and H.-R. Trebin, Molecular dynamics simulations of crack propagation in quasicrystals, in *Proceedings of the 6th International Conference on Quasicrystals, Tokyo 1997* (Edited by S. Takeuchi and T. Fujiwara), pages 485–492, (1998).

[6] H.-R. Trebin, R. Mikulla, J. Stadler, G. Schaaf, and P. Gumbsch, Molecular dynamics simulations of crack propagation in quasicrystals, *Comput. Phys. Commun.* **121 122** (1999) 536–539.

[7] D. Levine and P. J. Steinhardt, Quasicrystals: a new class of ordered structures, *Phys. Rev. Lett.* **53** (1984) 2477–2480.

[8] H.-R. Trebin, editor, *Quasicrystals. Structure and Physical Properties*, WILEY-VCH, (2003).

[9] P. Schall, *Plastizität dekagonaler Al-Ni-Co-Einkristalle*, Ph.D. thesis, Institut für Festkörperforschung, Forschungszenrum Jülich GmbH, (2002).

[10] L. X. He, X. Z. Li, Z. Zhang, and K. H. Kuo, One-Dimensional Quasicrystal in Rapidly Solidified Alloys, *Phys. Rev. Lett.* **61** (1988) 1116–1118.

[11] K. Chattopadhyay, K. S. Lele, S. Ranganathan, G. N. Subbanna, and N. Thangaraj, Electron microscopy of quasi-crystals and related structures, *Current Science* **54** (1985) 895.

[12] N. Wang, H. Chen, and K. H. Kuo, Two–dimensional quasicrystal with eightfold rotational symmetry, *Phys. Rev. Lett.* **59** (1987) 1010–1013.

[13] T. Ishimasa, H.-U. Nissen, and Y. Fukano, New Ordered State Between Crystalline and Amorphous in Ni–Cr Particles, *Phys. Rev. Lett.* **55** (1985) 511–513.

[14] A. P. Tsai, A. Inoue, Y. Yokoyama, and T. Masumoto, Stable icosahedral AlPdMn and AlPdRe alloys, *Mat. Trans. JIM* **31** (1990) 98–103.

[15] P. Sainfort and B. Dubost, The T2 compound: A stable quasicrystal in the system Al-Li-Cu-(Mg)?, *Journal Phys. France* **47** (1986) 321–330.

[16] B. Dubost, J. M. Tanaka, P. Sainfort, and M. Audier, Large AlCuLi single quasicrystals with triacontahedral solidification morphology, *Nature* **324** (1986) 48–50.

[17] A.-P. Tsai, A. Inoue, and T. Masumoto, A stable quasicrystal in Al-Cu-Fe system, *Jpn. J. Appl. Phys.* **26** (1987) L1505 L1507.

[18] A. P. Tsai, A. Niikura, A. Inoue, T. Masumoto, Y. Nishita, K. Tsuda, and M. Tanaka, Highly ordered structure of icosahedral quasicrystals in Zn-Mg-RE(RE≡rare earth metals) systems, *Phil. Mag. Lett.* **70** (1994) 169–175.

[19] K. F. Kelton, Ti/Zr-based quasicrystals-formation, structure and hydrogen storage properties, in *Mater. Research Society Samposium Proceedings* (Edited by J.-M. Dubois, P. A. Thiel, A. P. Tsai, and KUrban), volume 553, pages 471–481, (1999).

[20] I. R. Fisher, M. J. Kramer, Z. Islam, A. R. R. A. Kracher, T. Wiener, M. J. Sailer, A. I. Goldman, and P. C. Canfield, On the growth of decagonal Al-Ni-Co quasicrystals from the ternary melt, *Phil. Mag. B* **79** (1999) 425–434.

[21] A. P. Tsai, J. Q. Guo, E. Abe, H. Takakura, and T. J. Sato, A stable binary quasicrystal, *Nature* **408** (2000) 537–538.

[22] J.-M. Dubois, S. S. Kang, and Y. Massiani, Application of quasicrystalline alloys to surface coating of soft metals, *J. Non-Cryst. Solids* **153 & 154** (1993) 443–445.

[23] C. Berger, Electronic properties of quasicrystals experimental, in *Lectures on Quasicrystals* (Edited by F. Hippert and D. Gratias), Les éditions de physique, Les Ulis, (1994).

[24] J.-M. Dubois, Quasicrystals, *J. Phys. Cond. Mat.* **13** (2001) 7753–7762.

[25] K. Edagawa, Dislocations in quasicrystals, *Mater. Sci. Eng. A* **309-310** (2001) 528–538.

[26] M. Feuerbacher, C. Metzmacher, M. Wollgarten, K. Urban, B. Baufeld, M. Bartsch, and U. Messerschmidt, The plasticity of icosahedral quasicrystals, *Mater. Sci. Eng. A* **233** (1997) 103–110.

[27] R. Mikulla, P. Gumbsch, and H.-R. Trebin, Dislocations in quasicrystals and their interaction with cluster-like obstacles, *Phil. Mag. Lett.* **78** (1998) 369–376.

[28] C. Deus, B. Wolf, and P. Paufler, On the orientation dependence of crack-like failure formation near indentations on an icosahedral Al-Pd-Mn quasicrystal, *Phil. Mag. A* **75** (1997) 1171–1183.

[29] U. Köster, W. Liu, H. Liebertz, and M. Michel, Mechanical properties of quasicrystalline and crystalline phases in Al–Cu–Fe alloys, *J. Non-Cryst. Solids* **153 & 154** (1993) 446–452.

[30] P. Gumbsch and R. M. Cannon, Atomistic aspects of brittle fracture, *Mater. Res. Bull.* **25** (2000) 15–20.

[31] P. J. Steinhardt and S. Ostlund, *The Physics of Quasicrystals*, World Scientific, Singapore, (1987).

[32] P. A. Kalugin, A. Yu.Kitaev, and L. S. Levitov, $Al_{0.86}Mn_{0.14}$: a six-dimensional crystal, *JETP Lett.* **41** (1985) 145–149.

[33] V. Elser, The diffraction pattern of projected structures, *Acta Crystallogr. Sect. A* **42** (1986) 36–43.

[34] A. Katz and M. Duneau, Quasiperiodic patterns and icosahedral symmetry, *J. Phys. France* **47** (1986) 181–196.

[35] M. Baake, P. Kramer, M. Schlottmann, and D. Zeidler, Planar patterns with fivefold symmetrie as sections of periodic structures in 4-Space, *Int. J. Mod. Phys. B* **4** (1990) 2217–2268.

[36] G. Zeger, *Strukturuntersuchung dekagonaler Quasikristalle mittels numerischer Simulation von Channeling-Rückstreuprofilen*, Ph.D. thesis, Universität Stuttgart, (1999).

[37] D. Joseph, M. Baake, P. Kramer, and H. R. Trebin, Diffusion in 2D quasicrystals, *Europhys. Lett.* **27** (1994) 451–456.

[38] P. A. Kalugin and A. Katz, A mechanism for self-diffusion in quasicrystals, *Europhys. Lett.* **21** (1993) 921–926.

[39] K. Edagawa, K. Suzuki, and S. Takeuchi, High Resolution Transmission Electron Microscopy Observation of Thermally Fluctuating Phasons in Decagonal Al-Cu-Co, *Phys. Rev. Lett.* **85** (2000) 1674–1677.

[40] K. Edagawa, K. Suzuki, and S. Takeuchi, HRTEM observation of phason flips in Al-Cu-Co decagonal quasicrystal, *J. All. Comp.* **342** (2002) 271–277.

[41] F. Lançon and L. Billard, Two-dimensional system with a quasicrystalline ground state, *J. Phys. France* **49** (1988) 249–256.

[42] F. Lançon and L. Billard, Thermodynamical Properties of a Two-Dimensional Quasicrystal from Molecular Dynamics Calculations, *Europhys. Lett.* **2** (1986) 625–629.

[43] H.-R. Trebin, R. Mikulla, and J. Roth, Motion of dislocations in two-dimensional decagonal quasicrystals, *J. Non-Cryst. Solids* **153 154** (1993) 272–275.

[44] C. L. Henley and V. Elser, Quasicrystal structure of $(Al, Zn)_{49}Mg_{32}$, *Phil. Mag. B* **53** (1986) L59 L66.

[45] M. Wollgarten, M. Beyss, K. Urban, H. Liebertz, and U. Köster, Direct Evidence for Plastic Deformation of Quasicrystals by Means of a Dislocation Mechanism, *Phys. Rev. Lett.* **71** (1993) 549–552.

[46] J. P. Hirth and J. Lothe, *Theory of dislocations*, J. Wiley and Sons, New York, (1982).

[47] R. Mikulla, G. Schaaf, and H.-R. Trebin, Gamma-surfaces in quasicrystals, *Phil. Mag. Lett.* **79** (1999) 721–726.

[48] R. Thomson, Physics of fracture, *Solid State Physics* **39** (1986) 1–129.

[49] B. Lawn, *Fracture of brittle solids 2nd edn*, Cambridge Solid State Science Series, Cambridge University Press, (1993).

[50] G. C. Sih and H. Liebowitz, *Mathematical Theories of Brittle Fracture*, volume 2, pages 67–190, Academic Press, (1968).

[51] L. B. Freund, *Dynamic fracture mechanics*, Cambridge monographs on mechanics and applied mathematics, Cambridge University Press, (1998).

[52] J. R. Rice and R. Thomson, Ductile versus brittle behaviour of crystals, *Phil. Mag. A* **73** (1974) 73–97.

[53] J. R. Rice, Dislocation nucleation from a crack tip: an analysis based on the peierls concept, *J. Mech. Phys. Solids* **40** (1992) 239–271.

[54] G. Schoeck, Dislocation emission from crack tips, *Phil. Mag. A* **63** (1991) 111–120.

[55] P. Gumbsch, J. Riedle, A. Hartmaier, and H. F. Fischmeister, Controlling factors for the brittle-to-ductile transition in tungsten single crystals, *Science* **282** (1998) 1293–1295.

[56] M. L. Falk, Molecular-dynamics study of ductile and brittle fracture in model noncrystalline solids, *Phys. Rev. B* **60** (1999) 7062–7070.

[57] R. Thomson, C. Hsieh, and V. Rana, Lattice trapping of fracture cracks, *J. Appl. Phys.* **42** (1971) 3154–3160.

[58] W. A. Curtin, On lattice trapping of cracks, *J. Mater. Res.* **5** (1990) 1549–1560.

[59] J. E. Sinclair, The influence of the interatomic force law and of kinks on the propagation of brittle cracks, *Phil. Mag.* **31** (1975) 647–671.

[60] J. Riedle, P. Gumbsch, and H.-F. Fischmeister, Cleavage Anisotropy in Tungsten Single Crystals, *Phys. Rev. Lett.* **76** (1996) 3594–3597.

[61] R. Pérez and P. Gumbsch, Directional anisotropy in the cleavage fracture of silicon, *Phys. Rev. Lett.* **84** (2000) 347–5350.

[62] G. Michot, Fundamentals of silicon fracture, *Crystal Properties and Preparation* **17-18** (1988) 55–98.

[63] M. P. Allen and D. J. Tildesley, *Computer Simulation of Liquids*, Oxford Science Publications, (1987).

[64] F. F. Abraham, D. Brodbeck, R. A. Rafey, and W. E. Rudge, Instability dynamics of fracture: A computer simulation investigation, *Phys. Rev. Lett.* **73** (1994) 272–275.

[65] B. L. Holian and R. Ravelo, Fracture simulations using large-scale molecular dynamics, *Phys. Rev. B* **51** (1995) 11275–11288.

[66] S. J. Zhou, P. S. Lomdahl, R. Thomson, and B. L. Holian, Dynamic crack processes via molecular dynamics, *Phys. Rev. Lett.* **76** (1996) 2318–2321.

[67] S. J. Zhou, D. M. Beazley, P. S. Lomdahl, and B. L. Holian, Large-scale Molecular Dynamics simulations of three-dimensional ductile failure, *Phys. Rev. Lett.* **78** (1997) 479–482.

[68] M. Marder and J. Fineberg, How things break, *Phys. Today* (1996) 24–29.

[69] P. Gumbsch, S. J. Zhou, and B. L. Holian, Molecular dynamics investigation of dynamic crack stability, *Phys. Rev. B* **55** (1997) 3445–3455.

[70] M. Ludwig and P. Gumbsch, An empirical interatomic potential for B2 NiAl, *Modelling and Simulation in Materials Science and Engineering* **3** (1995) 533–542.

[71] M. Ludwig and P. Gumbsch, Cleavage fracture and crack tip dislocation emission in B2 NiAl: An atomistic study, *Acta Materialia* **46** (1998) 3135–3143.

[72] D. Farkas, Atomistic studies of intrinsic crack-tip plasticity, *Mater. Res. Bull.* **25** (2000) 35–38.

[73] W. T. Ashurst and W. G. Hoover, Microscopic fracture studies in the two-dimensional triangular lattice, *Phys. Rev. B* **14** (1976) 1465–1473.

[74] F. F. Abraham, R. Walkup, H. Gao, M. Duchaineau, T. D. D. L. Rubia, and M. Seager, Simulating materials failure by using up to one billion atoms and the world's fastest computer: Work-hardening, *Proc. Nat. Acad. Sci. U.S.A.* **99** (2002) 5783–5787.

[75] J. Stadler, R. Mikulla, and H.-R. Trebin, IMD: a software package for molecular dynamics studies on parallel computers, *Int. J. Mod. Phys. C* **8** (1997) 1131–1140.

[76] J. Roth, J. Stadler, F. Gähler, J. Hahn, M. Hohl, C. Horn, J. Kaiser, R. Mikulla, G. Schaaf, J. Stelzer, and H.-R. Trebin, *Molecular dynamics simulations with IMD*, 169-173, (1999).

[77] J. Roth, IMD — A Molecular Dynamics Program and Applications, in *Proceedings of the Workshop on Molecular Dynamics on Parallel Computers* (Edited by R. Esser, P. Grassberger, J. Grotendorst, and M. Lawerenz), page 83. World Scientific, Singapore, (2000).

[78] http://www.itap.physik.uni-stuttgart.de/~imd.

[79] G. Schaaf, *Numerical simulation of dislocation motion in icosahedral quasicrystals*, Ph.D. thesis, Institut für Theoretische und Angewandte Physik, Universität Stuttgart, (2002).

[80] G. Schaaf, J. Roth, and H.-R. Trebin, Dislocation motion in icosahedral quasicrystals at elevated temperatures: numerical simulation, *Phil. Mag. A* **83** (2003) 2449–2465.

[81] E. Bitzek, F. Gähler, J. Hahn, C. Kohler, G. Krdzalic, J. Roth, C. Rudhart, G. Schaaf, J. Stadler, and H.-R. Trebin, Recent developements in IMD: Interactions for covalent and metallic systems, in *High Performance Computing in Science and Engineering 2000* (Edited by E. Krause and W. Jäger), pages 37–47, Springer, Heidelberg, (2001).

[82] J. R. Rice, *Mathematical Analysis in the Mechanics of Fracture*, volume 2, pages 191–311, Academic Press, (1968).

[83] W. G. Hoover, Generalization of Nosé's isothermal molecular dynamics: Non-hamiltonian dynamics for the canonical ensemble, *Phys. Rev. A* **40** (1989) 2814–2815.

[84] D. J. Evans and B. L. Holian, The Nosé-Hoover thermostat, *J. Chem. Phys.* **83** (1985) 4069–4074.

[85] W. G. Hoover, Canonical dynamics: Equilibrium phase–space distributions, *Phys. Rev. A* **31** (1985) 1695–1697.

[86] B. L. Holian, A. Voter, and R. Ravelo, Thermostatted molecular dynamics: How to avoid the Toda demon hidden in Nosé-Hoover dynamics, *Phys. Rev. E* **52** (1995) 2338–2347.

[87] H. J. C. Berendsen, J. P. M. Postma, W. F. van Gunsteren, A. DiNola, and J. R. Haak, Molecular dynamics with coupling to an external bath, *Journal Chem. Phys.* **81** (1984) 3684–3690.

[88] M. Brede, K. J. Hsia, and A. S. Argon, Brittle crack propagation in silicon single crystals, *J. Appl. Phys.* **70** (1991) 758–771.

[89] B. J. Gally and A. S. Argon, Brittle-to-ductile transitions in the fracture of silicon single crystals by dynamic crack arrest, *Phil. Mag. A* **81** (2001) 699–740.

[90] M. W. Finnis, P. Agnew, and A. J. E. Foreman, Thermal excitation of electrons in energetic displacement cascades, *Phys. Rev. B* **44** (1991) 567–574.

[91] C. L. Henley, Random tiling models, in *Quasicrystals – The State of the Art* (Edited by D. P. DiVincenzo and P. J. Steinhardt), pages 429–524, World Scientific, (1991).

[92] J. E. Lennard-Jones, On the Determination of Molecular Fields. I. From the Variation of the Viscosity of a Gas with Temperature, *Proc. R. Soc. London, Ser. A* **106** (1924) 441–462.

[93] F. Lançon and L. Billard, Binary tiling tools for models, in *Lectures on Quasicrystals* (Edited by F. Hippert and D. Gratias), pages 265–279, Les Editiones de Physique, Les Ulis, (1994).

[94] H. K. Lee, R. H. Swendsen, and M. Widom, Crystalline ground states of an entropically stabilized quasicrystal model, *Phys. Rev. B* **64** (2001) 224201–224204.

[95] R. Mikulla, *Atomistische Studien zur Versetzungsbewegung in zweidimensionalen Quasikristallen*, Ph.D. thesis, Universität Stuttgart, (1996).

[96] S. Nosé, A Unified Formulation of the Constant Temperature Molecular Dynamics Methods, *J. Chem. Phys.* **81** (1984) 511–519.

[97] S. Nosé, A Molecular Dynamics Method for Simulations in the Canonical Ensemble, *Mol. Phys.* **52** (1984) 255–268.

[98] S. Nosé, An extension of the canonical ensemble molecular dynamics method, *Mol. Phys.* **57** (1986) 187–191.

[99] H. C. Andersen, Molecular dynamics simulations at constant pressure and/or temperature, *J. Chem. Phys.* **72** (1980) 2384–2393.

[100] S. J. Zhou, D. L. Preston, P. S. Lomdahl, and D. M. Beazley, Large-scale molecular dynamics simulations of dislocation intersection in copper, *Science* **279** (1998) 1525–1527.

[101] R. Mikulla, F. Krul, P. Gumbsch, and H.-R. Trebin, Numerical simulations of dislocation motion and crack propagation in quasicrystals, in *New horizons in quasicrystals: Research and applications* (Edited by A. I. Goldman, D. J. Sordelet, P. A. Thiel, and J. M. Dubois), pages 200–207. World Scientific, (1997).

[102] R. Mikulla, J. Stadler, P. Gumbsch, and H.-R. Trebin, Molecular Dynamics Simulations of Crack Propagation in Quasicrystals, in *Proceedings of the 6th International Conference on Quasicrystals* (Edited by S. Takeuchi and T. Fujiwara), pages 485–492. World Scientific, (1997).

[103] V. Vitek, Theory of the core structures of dislocations in body-centered-cubic metals, *Cryst. Latt. Def.* **5** (1974) 1–34.

[104] R. Mikulla, J. Roth, and H.-R. Trebin, Plastic behaviour of quasicrystals: Shearing a two-dimensional binary tiling model in a nonequilibrium–molecular–dynamics simulation, in *Proceedings of the 5th International Conference on Quasicrystals* (Edited

by Ch. Janot and R. Mosseri), pages 298–305. World Scientific, (1995).

[105] T. Egami, K. Maeda, and V. Vitek, Structural defects in amorphous solids - a computer simulation study, *Phil. Mag. A* **41** (1980) 883–901.

[106] D. Srolovitz, K. Maeda, V. Vitek, and T. Egami, Structural defects in amorphous solids - statistical analysis of a computer model, *Phil. Mag. A* **44** (1981) 847–866.

[107] M. L. Falk and J. S. Langer, Dynamics of viscoplastic deformation in amorphous solids, *Phys. Rev. E* **57** (1998) 7192–7205.

[108] F. Spaepen, Microscopic mechanism for steady-state inhomogeneous flow in metallic glasses, *Acta Metall.* **25** (1977) 407–415.

[109] A. S. Argon, Plastic deformation in metallic glasses, *Acta Metall.* **27** (1979) 47–58.

[110] M. L. Falk, *Deformation and Fracture in Amorphous Solids*, Ph.D. thesis, University of California, Santa Barbara, (1999).

[111] F. Rösch, *Numerische Studien zur Rissausbreitung in dreidimensionalen komplexen Kristallstrukturen*, Diplomarbeit, Universität Stuttgart, (2003).

[112] J. Roth, Shock waves in quasicrystals, *Ferroelectrics* **250** (2001) 365–368.

[113] J. Roth, Large-scale molecular dynamics simulations of shock waves in laves crystals and icosahedral quasicrystals, in *AIP Conf. Proc.*, volume 620, pages 378–384, (2002).

[114] G. D. Schaaf, J. Roth, H.-R. Trebin, and R. Mikulla, Numerical simulation of dislocation motion in three-dimensional icosahedral quasicrystals, *Phil. Mag. A* **80** (2000) 1657–1668.

[115] G. Bergman, J. L. T. Waugh, and L. Pauling, The crystal structure of the metallic phase $Mg_{32}(Al,Zn)_{49}$, *Acta Crystallogr.* **10** (1957) 254–259.

[116] M. Boudard and et.al., Neutron and x-ray single-crystal study of the AlPdMn icosahedral phase, *J. Phys. Cond. Mat.* **4** (1992) 10149–10168.

[117] W. Yang, K. Urban, and M. Feuerbacher, Cluster structure and low-energy planes in icosahedral Al-Pd-Mn quasicrystals, *Journal of Alloys and Compounds* **342** (2002) 164–168.

[118] L. Bresson, Mechanical properties of quasicrystals, in *Lectures on Quasicrystals* (Edited by F. Hippert and D. Gratias), Les Editions de Physique, Les Ulis, (1994).

[119] Y. Yokoyama, A. Inoue, and T. Masumoto, Mechanical properties, fracture mode and deformation behavior of $Al_{70}Pd_{20}Mn_{10}$ single-quasicrystal., *Mat. Trans. JIM* **34** (1993) 135–145.

[120] P. Paufler and B. Wolf, Deformation of quasicrystals by indentation, in: *Quasicrystals. Structure and Physical Properties*(Edited by H.-R. Trebin), pages 501–522, WILEY-VCH, (2003).

Index

Lebenslauf

Christoph Paul Rudhart geboren am 6. Juni 1972 in Friedrichshafen

Eltern:	Franz Joseph Rudhart und Barbara geb. Zahn
1979 - 1983	Besuch der Pestalozzi-Grundschule Friedrichshafen
1983 - 1989	Besuch der Graf-Soden-Realschule Friedrichshafen, Abschluß: Mittlere Reife
1989 - 1992	Besuch des Gymnasiums der dreijährigen Aufbauform – technische Richtung – an der Claude-Dornier-Schule Friedrichshafen, Abschluß: Allgemeine Hochschulreife
1992 - 1999	Studium an der Universität Stuttgart im Studiengang Lehramt an Gymnasien mit den Hauptfächern Mathematik und Physik, Staatsexamen in Mathematik und Physik
seit Juli 1999	Promotion bei Prof. Dr. H.-R. Trebin Institut für Theoretische und Angewandte Physik der Universität Stuttgart

Danksagung

An dieser Stelle möchte ich einigen Menschen danken, die zum Gelingen dieser Arbeit beigetragen haben.

Herrn Prof. Dr. Hans-Rainer Trebin danke ich für die freundliche Aufnahme am Institut für Theoretische und Angewandte Physik, sowie für die interessante, herausfordernde Aufgabenstellung und die Unterstützung bei ihrer Bearbeitung.

Herrn Prof. Dr. Hans Herrmann danke ich für die Übernahme des Mitberichts.

Herrn Prof. Dr. Peter Gumbsch vom Institut für Zuverlässigkeit von Bauteilen und Systemen der Universität Karlsruhe möchte ich für viele wertvolle Anregungen danken. Während meinen Besuchen bei ihm in Karlsruhe und Freiburg hatte er trotz seines sehr engen Zeitplans stets ein offenes Ohr für meine Probleme.

Dr. Franz Gähler und Dr. Johannes Roth danke ich für die Beantwortung vieler Fragen insbesondere zu Tilings, für die Unterstützung bei der Erzeugung der Modellquasikristalle und für die Hilfe bei der Implementierung der Erweiterungen des Simulationsprogramms IMD.

Meinem Kollegen Ulrich Koschella danke ich für die unzähligen Diskussionen über physikalische und weniger physikalische Themen. Unsere gemeinsamen Konferenzbesuche werden mir immer in bester Erinnerung bleiben.

Frohmut Rösch danke ich für seine Hilfe bei der Durchführung der Simulationen der Rissausbreitung in den ikosaedrischen Modellquasikristallen.

Ohne sie alle aufzuzählen bedanke ich mich bei den Mitarbeitern des ITAP und des Sekretariats für die angenehme Arbeitsatmosphäre und die schöne Zeit, die ich am Institut verbracht habe.

Ich danke meiner Freundin Sabine Fechter für die Unterstützung und ihren Zuspruch, sowie für die Übernahme des Korrekturlesens dieser Arbeit.

Meinen Eltern gilt mein ganz besonderer Dank dafür, dass sie mir meine Ausbildung ermöglicht haben.

Zuletzt danke ich der Deutschen Forschungsgemeinschaft, die im Rahmen des Schwerpunktprogramms 1031 (“Quasikristalle: Struktur und physikalische Eigenschaften”) diese Arbeit finanziell gefördert hat.